Received 16 February 2024; revised 30 March 2024; accepted 27 April 2024. Date of publication 6 May 2024; date of current version 24 September 2024.

Digital Object Identifier 10.1109/OJAP.2024.3397193

Sub-GHz Wrist-Worn Antennas for Wireless Sensing Applications: A Review

SANJEEV KUMAR[1] (Member, IEEE), GHOLAMHOSEIN MOLOUDIAN[1] (Member, IEEE), ROY B. V. B. SIMORANGKIR[2] (Member, IEEE), DINESH R. GAWADE[1] (Graduate Student Member, IEEE), BRENDAN O'FLYNN[1] (Senior Member, IEEE), AND JOHN L. BUCKLEY[1] (Member, IEEE)

[1]Tyndall National Institute, University College Cork, Cork, T12 K8AF Ireland

[2]Department of Engineering, Durham University, DH1 3LE Durham, U.K.

CORRESPONDING AUTHOR: S. KUMAR (e-mail: sanjeev.kumar@tyndall.ie)

This work was supported in part by the Science Foundation Ireland (SFI) as part of the SFI Centre VistaMilk under Grant SFI 16/RC/3835; in part by the CONNECT Centre for Future Networks and Communications under Grant 13/RC/2077; in part by the Insight Centre for Data Analytics under Grant SFI/12/RC/2289-2 and Grant 16/RC/3918-CONFIRM; in part by the Enterprise Ireland-funded Holistics Disruptive Technologies Innovation Fund (DTIF) under Grant EIDT20180291-A; and in part by the European Regional Development Fund.

ABSTRACT With recent advances in wearable wrist-worn wireless sensing applications, the demand for smartwatches and wristbands is rapidly increasing due to their widespread adoption in applications such as smart health monitoring, security, and fitness tracking. Currently, these devices primarily operate in the 2.45 GHz band, leveraging the availability of Bluetooth and Wi-Fi wireless technologies. However, the use of Sub-GHz frequencies (e.g., 433 MHz, 868 MHz, 915 MHz, 923 MHz) for wearable systems has also gained interest due to the emergence of wireless technologies like long-range wide area network (LoRaWAN), narrowband-IoT (NB-IoT) and Sigfox, which offer the potential for long-range wireless communications and sensing applications. In recent times, there has been a notable surge in the commercial production of a variety of Sub-GHz wrist-worn wireless sensing devices for health monitoring and tracking applications. Nevertheless, communications at Sub-GHz frequencies present significant challenges in antenna design, primarily due to the practical size constraints of wrist-worn devices and the necessity for using electrically small antennas. This paper meticulously reviews wrist-worn Sub-GHz antennas reported in the literature, analyzing key antenna parameters such as antenna topology, size, impedance bandwidth, peak realized gain, radiation efficiency, and specific absorption rate (SAR). Additionally, it underlines antenna design challenges, limitations, current trends, and presents potential future perspectives. To the best of the author's knowledge, there is currently no existing literature comprehensively reviewing Sub-GHz wrist-worn antennas. Therefore, this paper represents the inaugural effort to provide a comprehensive review in this specific domain.

INDEX TERMS Wireless sensing, wrist-worn, wristwear, wearable antenna, Sub-GHz, LoRaWAN, NB-IoT, Sigfox, smartwatch antenna, wristband.

I. INTRODUCTION

THE LAST few decades have seen a significant advancement in wireless sensor network (WSN) technology owing to its widespread use across an expanding range of applications, such as smart health monitoring, security, sports, fitness tracking, as well as localization and proximity alerting [1], [2]. When a WSN is specifically employed for the wireless networking of wearable and implantable sensors, it is referred to as a Wireless Body Sensor Network (WBSN) [3]. Furthermore, due to recent advances in WBSN and wearable technologies, smart wearable devices have started to appear in an ever-increasing number of applications, such as smartwatches [4], wristbands [5], smart clothing [6] and smart glasses [7] to name but a few. However, of these different groups of wearable devices, smartwatches are the most popular form factor for wearables

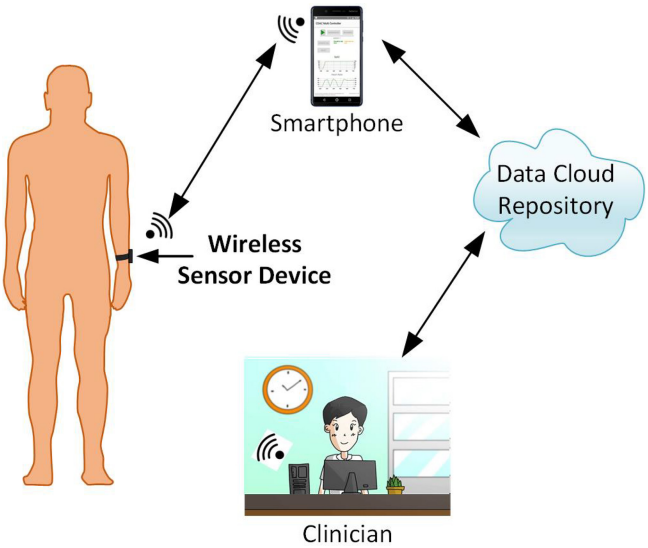

FIGURE 1. Overview of a typical WSN system for health monitoring [9].

mainly because of their ability to be worn seamlessly and conveniently on the human body and help the users to collect, analyze and wirelessly transfer real-time personal physiological data to external monitoring devices [2], [8].

Fig. 1 depicts a typical WSN system for health monitoring, featuring a wristwatch-based wireless sensor node. A wireless radio transceiver with one or more integrated antennas is a key component of a wireless sensor node because the radio transceiver enables sensor nodes to wirelessly communicate with external devices, such as smartphones [9], [11]. Further, the sensor data stored in a smartphone can be wirelessly forwarded to the data cloud repository via a wireless network such as Wi-Fi or cellular networks [12]. Once the measured data is available on the data cloud repository, the measured information can be easily accessed at a nurse station for further analysis of health records and planning treatments. The seamless integration of wearable devices into wireless health monitoring applications not only enhances real-time data accessibility but also streamlines healthcare processes, facilitating more informed decision-making and personalized patient care. The impact of wearable devices on wireless health monitoring, enabling real-time data accessibility and personalized care, is driving the continual growth of the global wearable technology market.

Fig. 2 shows the global wearable technology market size (in USD Billion) from 2022 to 2032 [10]. The Global Wearable Market is forecasted to witness remarkable expansion, with its value expected to reach about USD 231 Billion by 2032, a significant increase from the 2022 figure of USD 61.3 Billion. This growth is projected to occur at a Compound Annual Growth Rate (CAGR) of 14.60% during the forecast period spanning from 2023 to 2032. Furthermore, it is observed that among the various existing smart wearable devices (e.g., wristwear, eyewear & headwear, footwear, neck-wear, and body-wear), wrist-worn devices are shown to have the largest market share throughout the forecasted period. In 2022, the wrist-wear product segment dominated the global wearable technology market, contributing over 49.45% to the total revenue and emerging as the leading segment. The smartwatch market is projected to experience the fastest CAGR of 14.1% during the forecast period, potentially reaching a market size of USD 60.1 Billion by 2031 [13]. This is due to the fact that users are familiar with the concept and ease of wearing wrist-worn devices such as wristwatches that can be worn conveniently on the human body. Fig. 2 demonstrates that wrist-wear is the most preferred wearable Internet of Things (IoT) device among users. Moreover, it is predicted that wrist wearables will continue to dominate the global wearable market in the near future, encapsulating the idea that 'the future global wearables market is all about the wrist' [13]. As depicted in Fig. 3, smartwatches play a significant role in wireless monitoring of human activities such as sleep and workout patterns as well as estimating biomedical and physiological health parameters such as heart rate and blood oxygen saturation (SpO2) level and heart-related parameters using electrocardiogram (ECG) techniques [14], [17], [18]. Smartwatches enabled with sensing and wireless communication capabilities are becoming increasingly available as commercial products in a variety of configurations in recent times. For example, the Huawei GT 2 Pro Watch [19], Apple watch series 9 [14], Garmin Vivo active 4 [20], Fitbit Sense [21], Samsung galaxy watch active [22] and Fossil Gen 5 [23] are some of the popular smartwatches available to users at the present time.

The wireless transmission and reception capabilities of smartwatches are facilitated through the use of integrated radio transceivers and wearable antennas. A wearable antenna can be described as an antenna designed to be incorporated into clothing or worn on the human body [24]. When an antenna is designed for integration into a wrist-worn device, it is referred to as a wrist-worn or wrist-wear antenna. In recent years, wrist-worn antennas have gained attention in a growing range of application domains, such as defense, security, healthcare, proximity alert, sports, and fitness monitoring [1], [25]. To ensure user convenience and comfort, a small, compact form factor is desired for wrist-worn devices. For instance, a notable point of reference would be the Apple Watch Series 9 [14], which is a market leader in 2024. This Apple smartwatch measures a total dimension of 45 mm × 41 mm × 10.7 mm. The small form factor for smartwatches is a key desirable feature; therefore, a high level of integration is required to implement such devices, with decreasing space available to integrate key components such as an antenna, battery, sensor unit, processing unit, and radio board, as illustrated in Fig. 4(a). Furthermore, as depicted in Fig. 4(b), compact metal-bezel smartwatches emerge as a premier choice in wearable wireless technology [16]. Their metal frames not only enhance aesthetic appeal but also ensure durability,

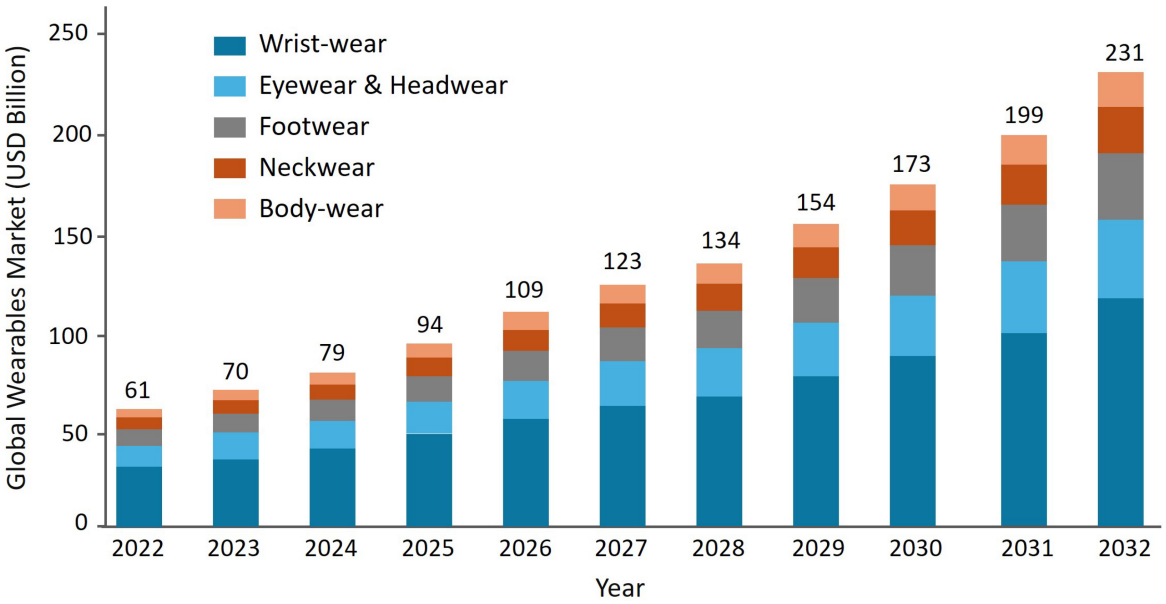

FIGURE 2. Global wearable technology market size (in USD Billion) from 2022 to 2032 [10].

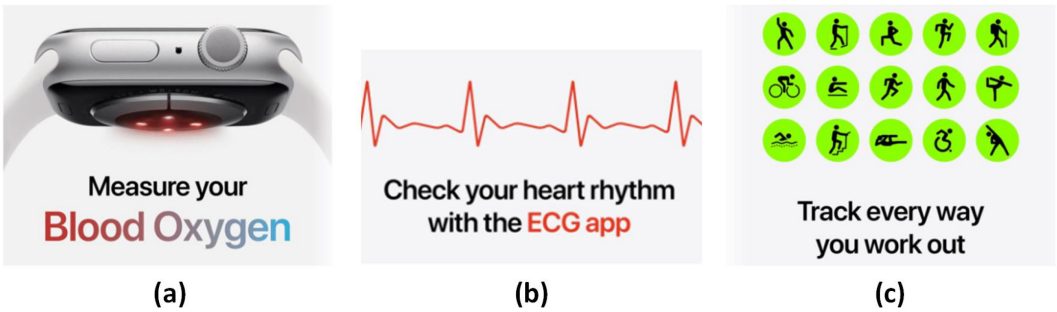

FIGURE 3. Biomedical applications of smartwatches in everyday life [14]: (a) SpO2 measurement, (b) electrocardiogram (ECG) monitoring, (c) Workout and activity tracking [14].

seamlessly blending style with resilience. Designing antennas for metal-bezel smartwatches presents a significant difficulty due to electromagnetic interference caused by the metal components, which can hinder antenna performance by blocking or reflecting radio signals [26].

The limited space allocated for integrating antennas in smartwatches necessitates the design of electrically small antennas. However, electrically small antennas have fundamental performance limitations in terms of impedance bandwidth, antenna gain, and radiation efficiency [27]. It is challenging to design high-performance antennas that can be accommodated within small-sized devices, especially at lower frequencies, such as Sub-GHz bands [28]. The communication range of a wireless device depends on the antenna gain [15]. As described in [29], a low-efficiency antenna results in reduced gain hence limited wireless communication range [15]. Maximizing antenna efficiency is therefore necessary to improve wireless communication range performance and extend battery lifetime [30]. Additionally, the design of wearable antennas is further complicated by the presence of the human body. When the human body is in close proximity to the antenna, the body tissue can absorb electromagnetic (EM) energy, leading to a reduction in antenna radiation efficiency and gain [31], [32].

In the literature, wrist-worn antennas operating across a range of frequencies have been reported, which can be summarized under two categories. Firstly, wrist-worn antennas for frequencies above 1 GHz, including antennas for the following frequencies: 1.575 GHz (Global Positioning System; GPS) [33], 2.45 GHz (ISM; IEEE 802.15.1, IEEE 802.15.4, and IEEE 802.11a/b/g) [34], 5.2 GHz (IEEE 802.11a/b/g) [35], 5.8 GHz (ISM; IEEE 802.11ac) [33], and 3.1–10.6 GHz (Ultra Wide Band; UWB) [36]. Currently, the majority of commercially available smartwatches are equipped with antennas for GPS, as well as 2.45 GHz Wi-Fi and Bluetooth technologies. The second category is referred to as wrist-worn antennas for Sub-GHz bands, which includes antennas for several frequency bands, including 402–405 MHz (Medical Implant Communication System; MICS) [37], 433 MHz (Industrial, Scientific, and Medical; ISM), 868 MHz (ISM in Europe) [38], and 915 MHz (ISM in North America) [39]. In the last decade, the use

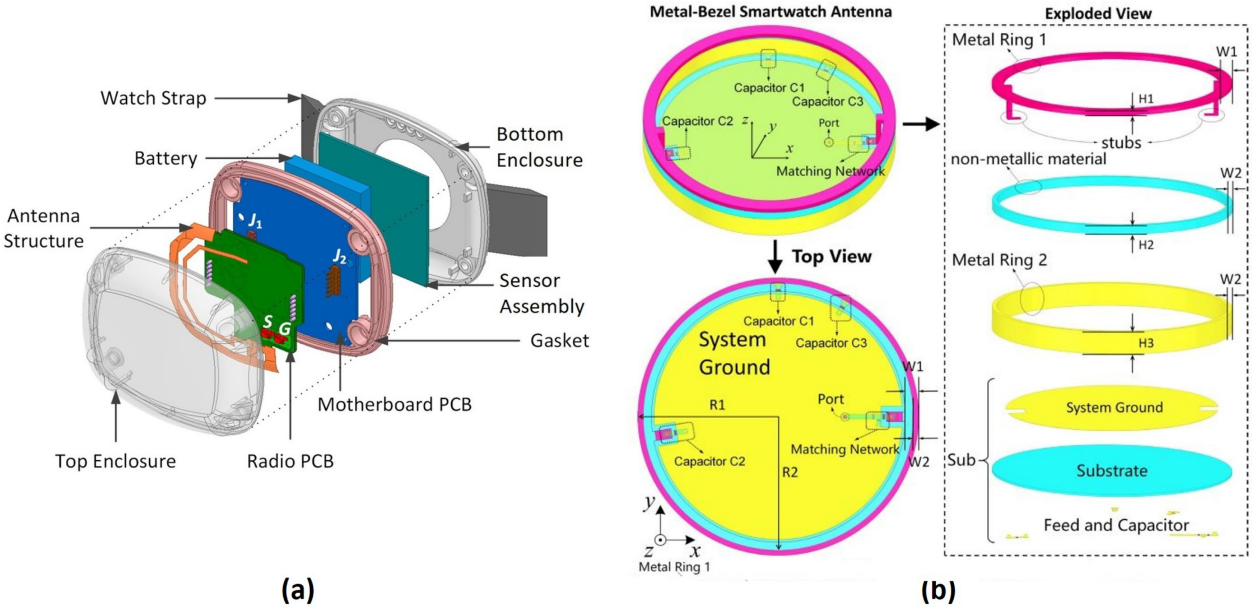

FIGURE 4. (a) Exploded view of a typical wristwatch wireless sensor device model [15], (b) Internal components of a typical metal-bezel smartwatch [16].

of Sub-GHz frequencies for wrist-worn wireless sensing systems has witnessed a growing interest due to the emergence of wireless technologies such as long- range wide area network (LoRaWAN) [40], narrowband-IoT (NB-IoT) [41], and SigFox [42], which have the potential for long-range wireless communications with low power operation and increased battery life [15], [39], [43], [44], [45]. This review paper focuses on analyzing Sub-GHz wrist-worn antennas reported in the literature, comparing key performance parameters, and highlighting design challenges, limitations, future trends, and perspectives.

The key contributions of this paper are outlined below:

- Significance of Sub-GHz Bands: This paper first outlines the key advantages of wireless communications at Sub-GHz frequencies such as 433 MHz, 868 MHz, and 915. Furthermore, it reviews commercially available Sub-GHz wrist-worn wireless sensor devices, highlighting the industry's interest in developing smartwatches enabled with LoRaWAN, NB-IoT, and Sigfox technologies to achieve long-range wireless communication with low power consumption.
- Sub-GHz Wrist-Worn Antennas: A comprehensive review of state-of-the-art Sub-GHz wrist-worn antennas reported in the existing literature is presented. The focus lies on analyzing key performance parameters of antennas and highlighting design challenges, limitations, ongoing trends, and future outlooks. Notably, there is a gap in the literature concerning reviews of Sub-GHz wrist-worn antennas. Therefore, this paper stands as the first endeavor to address this gap and provide a thorough review within this specific domain.
- Applications and Future Perspectives: The paper highlights the diverse application areas of Sub-GHz wrist-worn devices and explores potential prospects concerning innovative smartwatch-integrated antennas for next-generation wireless sensing solutions. The envisioned future prospects encompass the utilization of additive manufacturing technologies (e.g., 3D printing, inkjet printing), energy harvesting and wireless charging solutions, an investigation into transparent materials for antenna fabrication, as well as the significance of incorporating metamaterials and circular polarization (CP) characteristics to boost the performance of Sub-GHz wrist-worn antennas.

The remainder of the paper is organized as follows: Section II discusses the key advantages and challenges of wireless communications at Sub-GHz frequencies. Additionally, this section provides a review of commercially available Sub-GHz smartwatch-based wireless sensing devices is provided in this section. Building upon these fundamental insights, Section III offers a detailed examination of state-of-the-art Sub-GHz wrist-worn antennas, focusing on implemented antenna topologies and highlighting impedance and radiation characteristics. Section IV presents a detailed comparative analysis of the design and performance of various Sub-GHz wrist-worn antennas. The future perspective of wrist-worn antennas is discussed in Section V, and finally, Section VI presents the main conclusions of this work.

II. ADVANTAGES OF WIRELESS COMMUNICATIONS AT SUB-GHZ FREQUENCIES

At present, the majority of wristwatch devices use the 2.45 GHz license-free industrial, scientific, and medical (ISM) band [46] leveraging the widespread adoption of Bluetooth and Wi-Fi wireless technologies. This choice is driven by the compatibility of these technologies with the radios found in prevalent wireless devices such as smartphones, allowing seamless data communication without

TABLE 1. Sub-GHz frequency bands.

Wireless Technology	Sub-GHz frequency band (MHz)	Ref.
LoRaWAN	America: 915 Asia: 433, 866, 921.5 Europe: 868	[40]
NB-IoT*	America: 600, 700, 850 Asia: 700, 800, 850 Europe: 800, 900	[41]
Sigfox	America: 915 Asia: 866, 921.5 Europe: 868	[42]

* NB-IoT comprises multiple discrete Sub-GHz frequency bands such as B5, B8, B12-B14, B17-B20, B26, B28, B31, B71-B72, and B85 [41].

the need for additional infrastructure. However, emerging wireless technologies such as long-range wide area network (LoRaWAN) [40] and SigFox [42] are making use of the Sub-GHz ISM bands-specifically, 915 MHz (902-928 MHz) in North America and 868 MHz (863-870 MHz) in Europe [44]. Furthermore, Narrowband-IoT (NB-IoT) operates globally on various Sub-GHz bands, such as B5, B8, B12, B13, B18, B19, B20, B26, B28, B71, B85) [41]. These technologies are distinguished by their ability to facilitate long-range communication ($>$ 1 km) with low power consumption [45]. The popular Sub-GHz frequency bands for LoRaWAN, NB-IoT, and Sigfox technologies are summarized in Table 1.

Wireless communications at 2.45 GHz often experience a limited communication range ($<$20m) compared to Sub-GHz frequencies. This limitation is largely due to increased free space path loss (FSPL) and reduced radio frequency (RF) penetration through walls and buildings [47]. At higher frequencies, radio waves interact more with the molecules in materials, leading to greater RF attenuation than at lower frequencies [48]. Therefore, owing to their ability to penetrate obstacles and offer reliable connectivity, Sub-GHz wireless technologies are more suitable for indoor environments, such as hospitals and offices, even in densely constructed areas. Additionally, the widespread use of license-free 2.45 GHz ISM band, can result in coexistence issues [49] that may degrade wireless performance. This situation may necessitate, multiple re-transmissions of the same information, adversely affecting the battery life of devices like smartwatches that operate on the 2.45 GHz ISM band [49], [50]. On the other hand, Sub-GHz bands such as 868 and 915 MHz face less congestion, partly due to a restricted duty cycle (typically $\leq$ 1% [51]). This allows them to avoid the coexistence challenges prevalent in the 2.45 GHz band [45], [47], particularly in applications where high data rates are not a priority. In addition, the lower RF attenuation through walls and other obstacles at Sub-GHz frequencies means that a radio transceiver operating in these bands can achieve a longer communication range with less power compared to its counterparts at 2.45 GHz [52].

In recent developments, the demand for wristwatch-based applications featuring long-range wireless communication capabilities has surged, primarily driven by the need for broader coverage, low power consumption, and prolonged battery life. For example, patient health monitoring in a hospital building may require a long wireless communication range to cover the entire hospital building [43]. Given the limited space available on smartwatches for battery integration, these devices typically house small batteries with limited capacity. Consequently, minimizing power consumption is a critical design consideration to ensure extended device usability without frequent recharges [53]. Wireless technologies such as LoRaWAN, NB-IoT, and SigFox, which operate on Sub-GHz frequencies have the potential to meet the above-mentioned long-range wireless communications with low power operation and extended battery life [45]. Specifically, the LoRaWAN standard utilizes a star network topology [54], offering significantly improved wireless communication range with reduced infrastructure cost compared to 2.45 GHz-based technologies, such as Bluetooth Low Energy (BLE). While BLE adopts a mesh network topology necessitating multiple relay nodes for extended coverage [55] this approach invariably increases the complexity and network infrastructure cost [56].

A. COMMERCIAL SUB-GHZ SMARTWATCH SOLUTIONS

Over recent years, the market has witnessed a significant increase in the development of smartwatches and wristbands operating on Sub-GHz bands, tailored specifically for wireless biomedical healthcare and monitoring applications. Among the various Sub-GHz wireless technologies (e.g., LoRaWAN, NB-IoT, and Sigfox), LoRaWAN stands out as the most popular choice [57], [58], [59], [63], [64], [65], [66], [67], closely followed by NB-IoT (in Sub-GHz bands, such as B5, B8, B12, B13, B18, B19, B20, B26, B28, B71, B85) [60], [61], [68], [69] and Sigfox [62]. The photographs of several commercially available Sub-GHz smartwatches and wristbands are shown in Fig. 5. Smartwatches and wristbands in [57], [58], [59], [63], [64], [65], [66], [67] harness the power of LoRaWAN connectivity to provide an array of health-related functionalities, including monitoring ambient temperature, body surface temperature, exercise tracking, heart rate, blood oxygen levels, sleep status, as well as offering robust tracking and alarm-raising capabilities. The popularity of LoRaWAN in this domain can be attributed to its extensive coverage range, low power consumption, and cost-effectiveness. Smartwatches in [60], [61], [68], [69] leverage NB-IoT technology, offering similar health monitoring features with the added benefit of leveraging existing cellular infrastructure for connectivity, ensuring reliable communication in urban and indoor environments. Furthermore, Sigfox-based smartwatch in [62] provides comparable functionalities while capitalizing on Sigfox's ultra-low-power and cost-effective characteristics, making it suitable for applications requiring long battery life and minimal data transfer. It is important to emphasize that

FIGURE 5. Commercial Sub-GHz band smart wrist-worn devices: (a) HKT: SW-200 LoRaWAN Smartwatch: [57], (b) Lilygo: T-Watch S3 LoRaWAN smartwatch [58], (c) Origo: ED20W LoRaWAN smartwatch [59], (d) Oviphone: B2315 NB-IoT Smart Wristband [60], (e) Kotonlink: KT-PW11 NB-IoT Smartwatch [61], (f) Sigfox partner network: Co-assist alert watch [62].

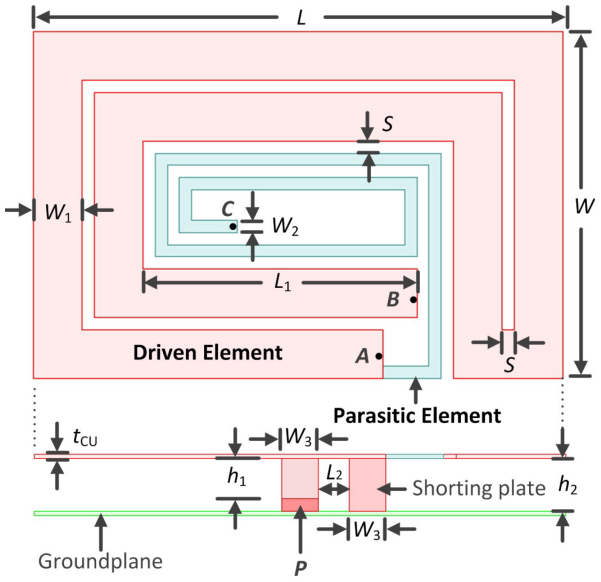

FIGURE 6. Configuration of the 915 MHz wristwatch PIFA antenna in [77].

commercial smartwatch manufacturers often refrain from disclosing details about the antennas integrated into their products. This reluctance is likely influenced by a variety of factors, including the need to maintain a competitive edge, the technical complexity involved, marketing strategies, regulatory compliance considerations, and the protection of proprietary technology.

III. STATE-OF-THE-ART SUB-GHZ WRIST-WORN ANTENNAS

Smart wrist-worn devices utilize integrated antennas to wirelessly communicate with external devices, such as smartphones and gateways, facilitating seamless data exchange and wireless health monitoring capabilities [15]. Designing antennas for these devices at Sub-GHz frequencies presents considerable challenges due to the constrained space available for antenna integration and the necessity to maintain key antenna performance metrics, such as impedance bandwidth, antenna gain, radiation efficiency, and specific absorption rate (SAR) [27], [70]. This review delves into the state-of-the-art in Sub-GHz wrist-worn antennas, showcasing their design strategies, performance considerations, and the latest advancements that are pushing the boundaries of what's possible in smartwatch and wristband technology, especially in the context of IoT healthcare and monitoring applications.

One of the earliest Sub-GHz wrist worn antennas was reported in 1984 [71], which was a loop antenna embedded in a wristwatch strap for FM radio reception (88 – 108 MHz) [72]. In the past years, this has evolved into diverse forms of antenna topologies, including planar Inverted-F antennas (PIFA) [15], [37], [39], [70], [73], [74], [75], [76], [77], [78], [79], [80], Inverted-F antennas (IFA) [81], [82], dipoles [83], [84], [85], [86], [87], monopoles [88], [89], [90], loops [38], [91], [92], helical antennas [93], [94], spiral antennas [95], and microstrip patch antennas [96], [97], [98], [99]. In the literature, various Sub-GHz wrist-worn antennas have been reported, with the majority of them accounting for the effects of the human body on antenna performance. However, a few papers neglect the presence of the human body, and the antenna parameters, such as impedance bandwidth, antenna gain, and efficiency are reported for free-space conditions [100], [101], [102], [103], [104]. It is important to highlight that this study only includes antennas that consider the effects of the human body on antenna performance. Those antennas designed only for free-space conditions are omitted, as they do not accurately represent real-world scenarios.

It is observed that PIFA and IFA antennas are the most widely used topologies for Sub-GHz wristwatch antennas due to their suitability for integration into low-profile, compact-size wristwatch devices. Additionally, the ground plane inherent to PIFA and IFA structures acts as a shield against backward radiation towards the human wrist, thereby reducing radiation losses into the wrist tissues [29], [37]. In [77], a novel 915 MHz wristwatch PIFA antenna using a dual-radiator approach for impedance bandwidth enhancement is presented. The antenna configuration is illustrated in Fig. 6 which measures a total size of 43.5 mm × 28.5 mm × 10.3 mm. This paper marks the first instance of utilizing dual radiators for enhancing the impedance bandwidth of a Sub-GHz wristwatch antenna. A dual radiator approach was employed to modify the input impedance, thereby enhancing the impedance matching of the antenna across the required band for 915 MHz operations (i.e., 902 - 928 MHz) [44], [105], [106]. When compared to the scenario with a single radiating element (driven element only), the inclusion of the second radiating element (parasitic element), resulted in an improvement of over 100% in

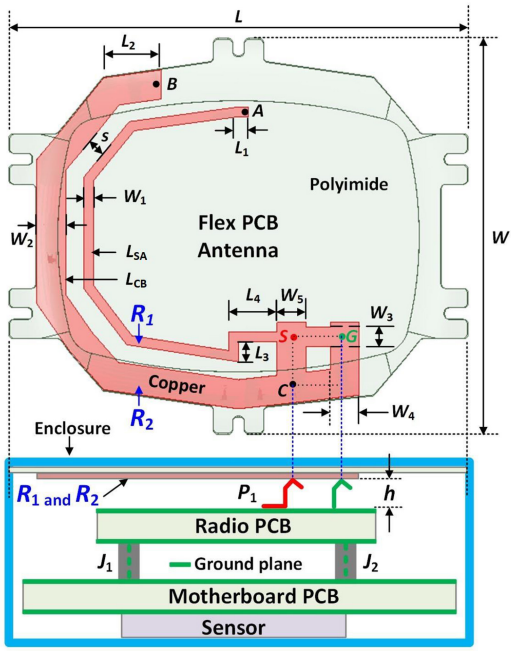

FIGURE 7. Configuration of the 915 MHz wristwatch-integrated PIFA antenna in [75].

the −10 dB impedance bandwidth. The measurements on the prototype antenna demonstrated a measured −10 dB impedance bandwidth of 26.4 MHz. Additionally, this antenna exhibited an on-phantom measured peak-realized gain of −0.57 dBi, and a simulated radiation efficiency of 46.8% at 915 MHz. Notably, for an input power of 1 mW, the antenna showcased a low peak Specific Absorption Rate (SAR) figure of less than 0.1% of the legal SAR limit of 4 W/kg averaged over 10-g of limb tissue mass [107], [108] ensuring both effectiveness in communication and safety in terms of human exposure to electromagnetic fields.

A compact wristwatch-integrated 915 MHz PIFA antenna, printed on a low-cost flexible polyimide substrate for wireless health monitoring applications is reported in [75]. The antenna configuration is illustrated in Fig. 7, where the antenna design employs dual-resonator elements denoted R_1 and R_2. An unbalanced antenna feed is provided using gold-plated spring-loaded contacts with the Signal and Ground connections denoted S and G respectively. The copper trace section between S and G is used to introduce an inductive shunt element, facilitating impedance matching to a 50-Ω source impedance. When measuring the antenna height from the nearest ground plane, this antenna occupies an overall dimension of 48 mm × 41 mm × 2.3 mm. Fig. 7 also depicts the internal components and stack-up of the wristwatch-based wireless sensor device. As shown, the antenna element can be attached to the enclosure lid and the radio and motherboard PCBs together serve as a ground plane for the PIFA topology. The prototype antenna exhibits a −10 dB impedance bandwidth of 30 MHz, a peak realized gain of −4.9 dBi, and a peak radiation efficiency of 15.9% at 915 MHz. Additionally, the antenna exhibits a very low SAR value of 0.003 W/kg, making it well-suited for various wrist-worn wireless applications.

Laser Direct Structuring (LDS) is a technology that enables the precise deposition of metal onto plastic parts through laser activation, allowing the direct printing of high-conductive nickel and gold-plated metal to implement antennas and RF components onto the surface of 3D plastic parts. The key benefit of LDS technology for antenna fabrication lies in its ability to create lightweight, compact, cost-effective, and highly customized antenna integration [109]. In [15], the 915 MHz antenna design reported in [75] was optimized for operation in the 868 MHz band. The 868 MHz antenna was manufactured by directly printing the antenna structure on the inner surface of an Acrylonitrile Butadiene Styrene (ABS) plastic enclosure using LDS technology. The use of LDS technology for antenna prototyping enabled low-cost, easy integration into the enclosure and eliminated the need for an additional flex PCB. Furthermore, this LDS-printed antenna incorporates a π-type impedance matching network to improve antenna performance by minimizing reflection and enhancing the impedance bandwidth. The on-phantom antenna measurement shows a −10 dB impedance bandwidth of 36 MHz. Additionally, with a peak realized gain of −4.86 dBi, a radiation efficiency of 14.53%, and a SAR figure of 0.003 W/kg at 868 MHz, this LDS antenna exhibits identical radiation performance to that of the 915 MHz antenna in [75].

The input impedance of an antenna is a critical design aspect that significantly influences its performance metrics, such as the reflection coefficient, bandwidth, and quality factor [110]. By fine-tuning the feedline geometry and dimensions, one can effectively control the impedance response of an antenna. For example, the feed structure of the 915 MHz antenna in [75] is optimized to control the impedance response thereby significantly improving the impedance bandwidth of the antenna. With the optimized feed structure, the antenna presented in [70] demonstrates a 107% bandwidth improvement compared to the antenna in [75]. As shown in Fig. 8, the antenna in [70] comprises two radiating elements, denoted Rad_1 and Rad_2, resembling the topology of a PIFA antenna in [15], [75]. The optimized feed structure enables the excitation of two closely located resonant modes, each independently tuned to maximize the impedance bandwidth [111]. Additionally, this paper introduces an equivalent transmission line model for the antenna to precisely explain the underlying mechanisms contributing to the antenna's impedance performance enhancements. On-phantom measurements of the prototype antenna show a −10 dB impedance bandwidth of 62 MHz, demonstrating a more than 100% improvement compared to the antenna in [75]. Although this antenna achieves a significant enhancement in impedance bandwidth, with a peak realized gain of −4.6 dBi, a radiation efficiency of 17.8%, and a SAR of 0.002 W/kg at 915 MHz, it demonstrates similar radiation performance to that of the

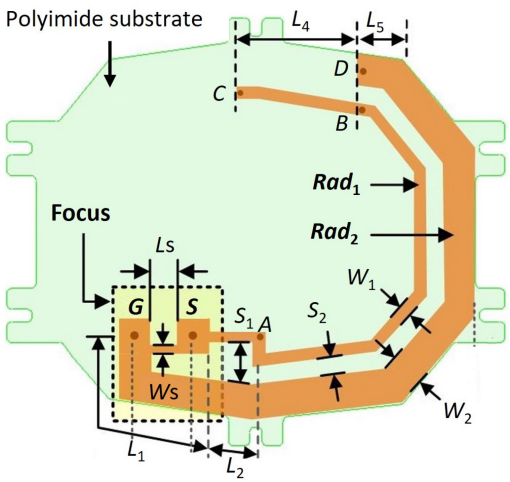

FIGURE 8. Configuration of the 915 MHz wristwatch PIFA antenna in [70].

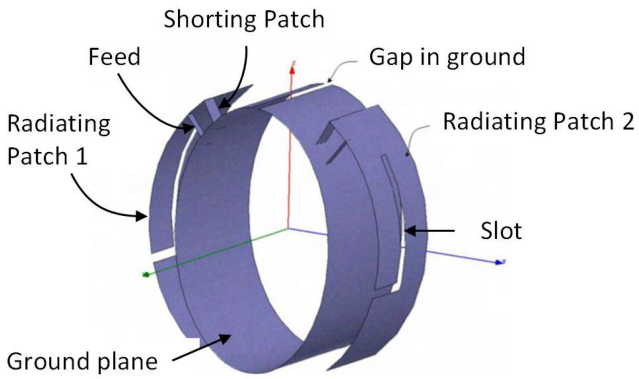

FIGURE 9. A novel wristwear dual-band diversity PIFA antenna [76].

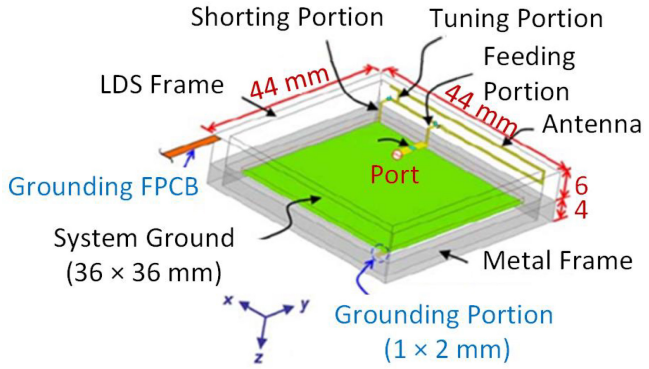

FIGURE 10. Integrated LDS metal frame PIFA antenna [74].

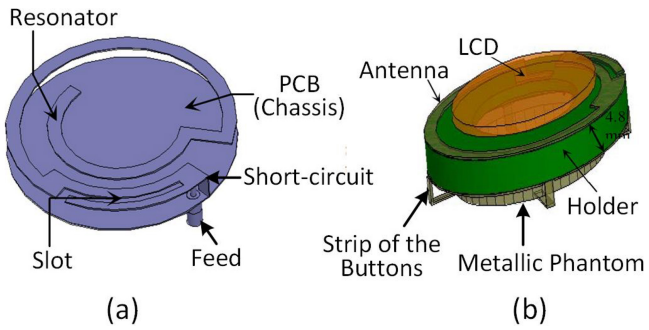

FIGURE 11. (a) PIFA Antenna structure, (b) Configuration of the casing watch [37].

antenna reported in [75]. A wrist-worn dual-band diversity PIFA antenna operating at 880 MHz and 1.8 GHz is reported in [76]. As shown in Fig. 9, the antenna comprises two PIFA-type radiating patches (Radiating patches 1 and 2), where dual-resonant operation is achieved by creating an L-shaped slot in the radiating patches. Both radiating elements share a common ground plane, and a gap in the ground plane is used to improve the isolation between the two radiating elements. This antenna has a −10 dB impedance bandwidth of 28 MHz and achieves a radiation efficiency of 83.7% at 880 MHz. However, the antenna has a large size of 188 mm × 30 mm × 6 mm which poses a significant challenge for integration into compact wristwatch devices.

A watch frame PIFA antenna capable of operating in the 746–787 MHz and 1710–2170 MHz bands is reported in [74]. As shown in Fig. 10, the wristwatch comprises a metal and laser direct structure (LDS) frame, together occupying a total volume of 44 mm × 44 mm × 6 mm. The antenna is printed inside the LDS frame, which is made of plastic with a relative electrical permittivity of $\epsilon_r = 2.92$ and a loss tangent of $tan\delta = 0.007$. The metallic part of the frame is connected to the PCB system ground. For this antenna, operation in the lower frequency band (746–787 MHz) is achieved by the LDS antenna in conjunction with the grounding flexible printed circuit board (FPCB), denoted as FPCB (connected to the metal frame), and an impedance matching capacitor. Conversely, operation in the higher frequency band (1710–2170 MHz) is accomplished with the help of a position-adjustable tuning portion. This watch frame PIFA antenna achieves a −10 dB impedance bandwidth of 35 MHz by incorporating a lumped capacitor (3.9 pF) in series with the feedline to match the input impedance of the antenna. Furthermore, this antenna has a peak realized gain of −5.4 dBi and radiation efficiency of 13% at $f_0 = 767$ MHz.

A spiral-shaped PIFA antenna for the MICS band (402-405 MHz) and Bluetooth (2.4-2.483 GHz) applications is reported in [37]. As depicted in Fig. 11(a), the antenna features a circular ground plane with a spiral resonator positioned 5 mm above the ground plane. The total spiral length is approximately one quarter-wavelength at 402.5 MHz, and a quarter-wavelength slot on the radiator's surface is added to excite resonance at 2.4 GHz. In Fig. 11(b), the wristwatch case configuration is illustrated, with the antenna holder constructed from Epoxy FR-4 substrate with $\epsilon_r = 4.4$ and $tan\delta = 0.01$, while the LCD is made of silicon substrate with $\epsilon_r = 11.9$. When worn on the user's arm, the proposed antenna demonstrates a −6 dB impedance bandwidth of 5.2 MHz, a peak realized gain of −12 dBi, and a radiation efficiency of 3.6% in the MICS band.

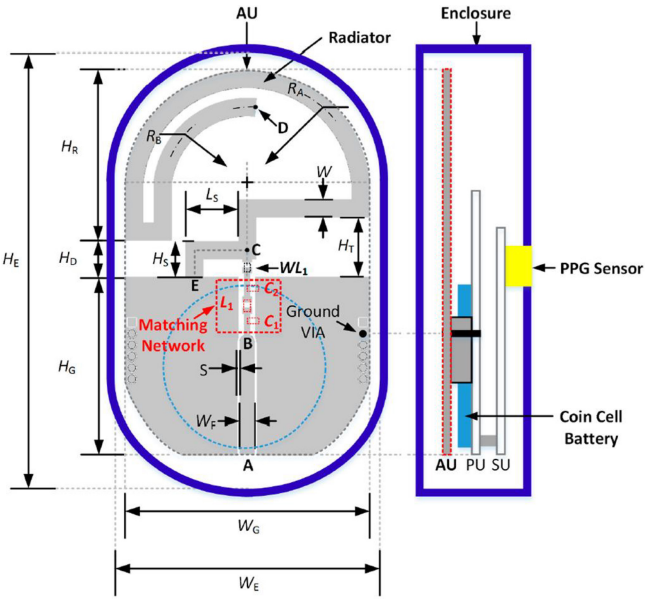

FIGURE 12. Geometry of the meandered 915 MHz PIFA [39].

As depicted in Fig. 12, a grounded coplanar waveguide (GCPW) fed meandered 915 MHz PIFA antenna designed for integration into a practical wristwatch-type sensor device for wireless health monitoring is presented in [39]. The antenna is realized using a standard FR-4 substrate material and has a compact size of 44 mm × 28 mm × 1.6 mm. The antenna incorporates an impedance-matching network to meet the demanding bandwidth requirements of 26 MHz for 915 MHz band operations. This antenna achieves a peak realized gain of −6.1 dBi at 915 MHz and with the help of a π-type matching network, a −10 dB impedance bandwidth of 55 MHz is achieved.

A multi-element wristwatch-integrated IFA antenna operating in the 810–960 MHz, 1370–1450 MHz, and 1710–2630 MHz bands is reported in [73]. As shown in Fig. 13, the proposed antenna features multiple radiating elements that are excited at different resonant frequencies, including 866 MHz, 1437 MHz, 1960 MHz, and 2300 MHz. At 866 MHz, the antenna exhibits a −10 dB impedance bandwidth of approximately 105 MHz, a peak realized gain of −4.4 dBi, and a radiation efficiency of 26%. Furthermore, for an input power of 22.96 dBm, this antenna demonstrates a 10-g SAR value of 0.78 W/kg at 836.5 MHz. However, it should be noted that the radiating part of the antenna in [73] extends to the strap of the wristwatch device. Furthermore, the width of the watch strap is also substantial, measuring 50 mm, which is not ideal for a practical wristwatch device in terms of comfort.

Another multi-element wrist-wearable three-antenna system for Long-Term Evolution (LTE) cellular and Global Positioning System (GPS) applications is reported [81]. The antenna configuration is depicted in Fig. 14, with overall dimensions of 93 mm x 37 mm x 5 mm. The antenna system (ANT1, ANT2, and ANT3) is integrated within an

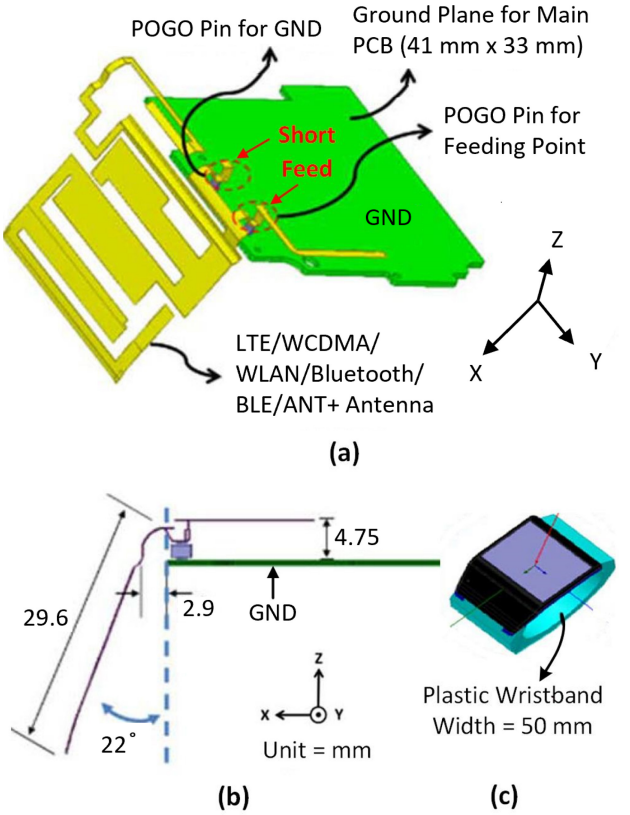

FIGURE 13. (a, b) Configuration of the wristwatch IFA, (c) Wristwatch model [73].

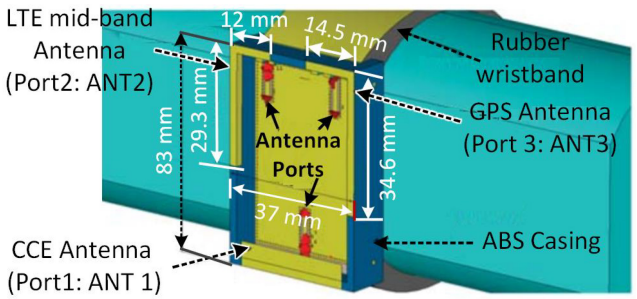

FIGURE 14. Configuration of the multiple-antenna system [81].

ABS plastic enclosure with $\epsilon_r = 2.7$ and $tan\delta = 0.005$. ANT1 is designed based on the Theory of Characteristic Mode and employs a capacitive coupling element to excite the fundamental chassis mode of the wristwatch device. The chassis ground extends to the wristband of the watch device to increase the electrical length of antenna ANT1 and incorporates a matching circuit to achieve resonance for LTE low-band (699-862 MHz) operation. The two Inverted-F antennas located on the top edge of the wristwatch case, denoted ANT2 and ANT3 in Fig. 14, are used for LTE mid-band (1710-2155 MHz) and GPS bands (1563-1605.7 MHz), respectively. The LTE low-band antenna (ANT1) has a radiation efficiency of 7.9% at 780 MHz and achieves a −10 dB impedance bandwidth of 105 MHz using an impedance-matching network.

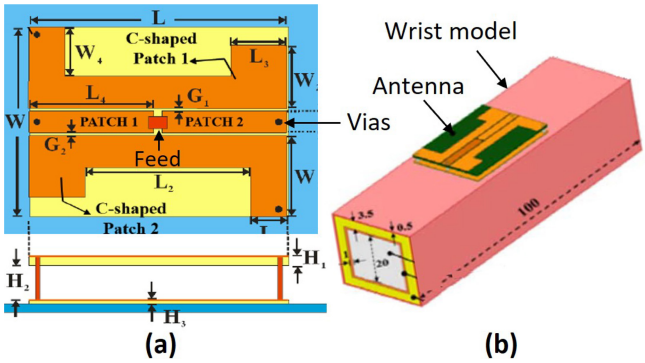

FIGURE 15. (a) Geometry of the 925 MHz 3D-dipole RFID tag antenna, (b) Tag antenna placed on a human wrist model [86].

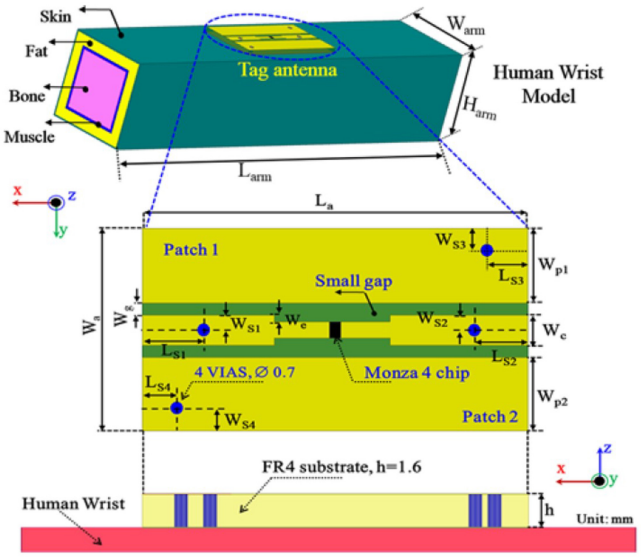

FIGURE 16. Geometry of the 915 MHz 3D-dipole RFID tag antenna reported in [87].

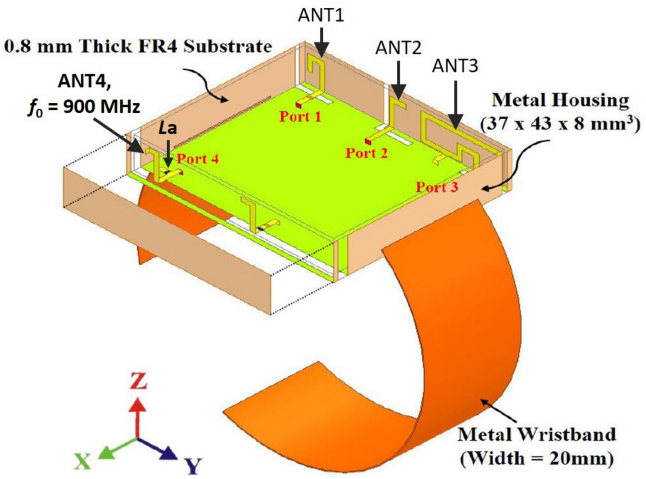

FIGURE 17. Geometry of the proposed antenna system [88].

Different variants of dipole and monopole antennas have been used for wrist-worn applications. For example, in [86], a compact 3D-dipole antenna designed for 925 MHz RFID on-wrist applications is presented. The structure of the proposed dipole RFID tag antenna is depicted in Fig. 15(a), and Fig. 15(b) shows the antenna positioned on a wrist model. The 3D-dipole antenna has overall dimensions of 32 mm × 25 mm × 3.2 mm and consists of two identical rectangular FR4 PCB layers separated by an air layer of $H_2 = 2$ mm. The upper layer is a 1 mm thick single-sided FR4 substrate, with a dipole formed by two rectangular patches (Patch 1 and Patch 2) and a pair of C-shaped patches on either side of the dipole. The lower FR4 layer, with a thickness of 0.2 mm, serves as the ground plane. Between the two FR4 layers, four shorting pins with a radius of 0.5 mm have been inserted at each end of the central rectangular strips and C-shaped strips to increase the antenna's current path. Additionally, the length L_2 and width W_2 of the C-shaped strips can be adjusted to modify the inductance of the antenna and match the antenna's impedance to that of the conjugate chip impedance. The antenna exhibits a narrow −10 dB impedance bandwidth of 6 MHz, and at 925 MHz, this antenna achieves a peak realized gain of −3.4 dBi and a radiation efficiency of 18%.

Fig. 16 illustrates the configuration of a compact wrist-worn dipole antenna designed for UHF RFID applications [87]. The antenna is printed on a FR4 substrate with total dimensions of 40 mm × 20 mm × 1.6 mm. The optimized antenna design consists of a dipole structure at the center, along with two additional closely coupled patches denoted as Patch 1 and Patch 2, situated near the radiating edges of the dipole. Four shorting pins, each with a radius of 0.7 mm are strategically positioned at both ends of the dipole as well as on the two coupled patches. This arrangement aims to produce a 3D dipole current flow directed through the top radiating plane to the ground, thereby increasing the resonant current path length and thus significantly minimizing the overall dimensions of the antenna. Furthermore, precise adjustment of via positions (i.e., LS_1, LS_2, LS_3, and LS_3) in combination with the width of the closely coupled patches (Wp1 and Wp2), or the small gap (Wg enables the tuning of the inductance in the proposed antenna to achieve perfect impedance matching with the conjugated impedance of the RFID chip. This UHF RFID dipole antenna demonstrated a −10 dB impedance bandwidth of 9 MHz, a peak realized gain of −3.2 dBi and a radiation efficiency of 14% at 915 MHz.

A multiple-antenna system for integration into a smart-watch device for Fifth-Generation Communications is reported in [88]. Fig. 17 illustrates the geometry of the proposed wristwatch-integrated antenna system and measures the total dimensions of 37 mm x 43 mm x 8 mm. The antenna system consists of four antenna units denoted as ANT1, ANT2, ANT3, and ANT4. ANT1 and ANT2 together form a MIMO system and operate at the 5G frequency range between 3.3 GHz to 5 GHz, ANT3 operates at WLAN 2.4-GHz/5-GHz dual-band. ANT4, which is fed at Port 4,

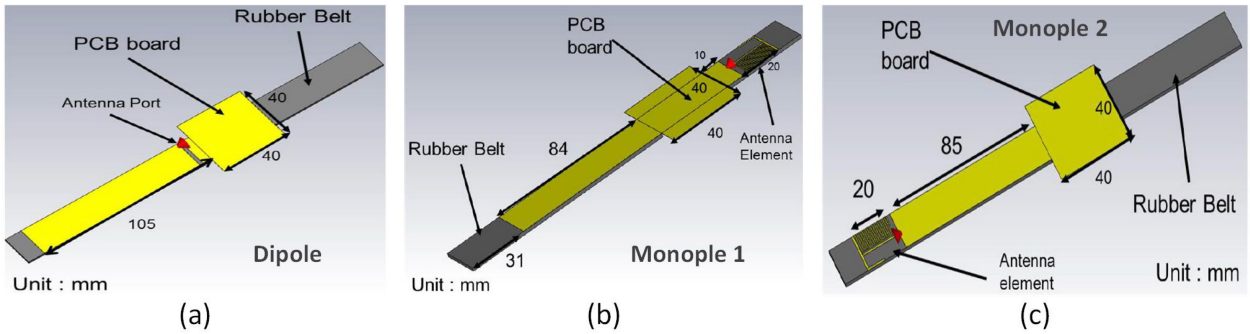

FIGURE 18. Geometry of the wristwatch antennas: (a) Dipole antenna, (b) Monopole antenna 1 and (c) Monopole antenna 2 in [84].

has a monopole topology and is optimized for operation at GSM 850/900, NB-IoT band (880-915 MHz), and GPS (1575 MHz). In ANT4, a lumped inductance $La = 3.9$ nH is used to control the impedance matching of the dual resonance mode generated in the GSM 850/900 band. This GSM antenna demonstrates a -10 dB impedance bandwidth of 95 MHz and a free-space peak realized gain of 1.2 dB at 900 MHz. Furthermore, when worn on a human wrist tissue model, ANT4 exhibits a maximum radiation efficiency of 30% in the frequency range of 820 MHz - 960 MHz and 10-g SAR figures of 0.25 W/kg and 0.54 W/kg, respectively, at 820 MHz and 930 MHz.

For a wrist-worn dipole antenna, the radiating element can be extended to the strap of a wristwatch to take advantage of the additional antenna real-estate provided by the wristwatch strap [83], [84], [112]. For example, in [84], a dipole and two types of monopole smartwatch antennas using a metallic strap operating in the frequency range of 0.7 GHz to 2.7 GHz are presented. As shown in Fig. 18, all antenna designs are realized using a copper metallic strip integrated into the rubber strap. The two dipole arms are formed using the metal conductor integrated into the strap and the PCB board ground plane, as shown in Fig. 18(a). Monopole 1 and Monopole 2 have similar configurations but are realized at different locations on the rubber belt, as depicted in Fig. 18(b, c). The dipole antenna exhibits a -10 dB impedance bandwidth of approximately 160 MHz at a frequency $f_0 = 750$ MHz, but it has a radiation efficiency of less than 9% at 750 MHz and less than 6.3% at 900 MHz. The close proximity of the radiating elements to the lossy human wrist tissue leads to the absorption of RF power in the human body, thereby limiting the radiation efficiency of the antenna. Specific Absorption Rate (SAR) is a measure of the rate at which RF power is absorbed by the human body when exposed to EM radiation [113], [114]. For 24 dBm input power, the dipole antenna in [84] demonstrated a 10-gram SAR value of 0.18 W/kg at 900 MHz, which is less than 5% of the maximum limit of 4.0 W/kg [107], [115].

The antenna in [112] presents the design of a metamaterial-based flexible dipole antenna for wrist-worn 910 MHz UHF RFID tag applications. As depicted in Fig. 19, this metamaterial-based antenna features a meander

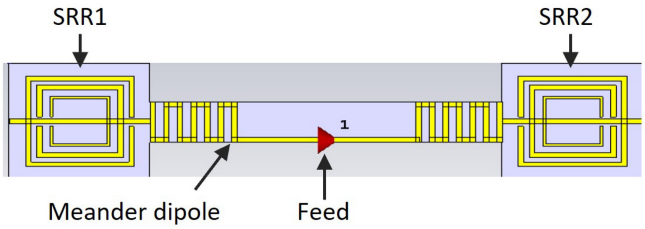

FIGURE 19. Geometry of the proposed metamaterial based 910 MHz UHF RFID tag antenna [112].

dipole topology with two split-ring resonator (SRR) cells denoted as SRR1 and SSR2. The antenna is designed using a flexible 0.277 mm thick photo paper substrate and silver trace as the conductive element, covering a total size of 117 mm x 26 mm. The antenna's performance is investigated under various bending conditions, specifically at 25°, 45°, and 60°. This paper presents only the simulated results, and for the on-body scenario, the antenna exhibits optimal impedance matching at a bending angle of 45°. The proposed on-body tag antenna achieves a -6 dB impedance bandwidth of 27 MHz, a peak realized gain of -11.87 dBi, and a radiation efficiency of 45%. Additionally, the antenna, without the SRR structures shows a peak realized gain of -12.43 dBi. It can therefore be seen that the inclusion of the metamaterial structures results in a realized gain improvement of 0.56 dBi.

In [83], an example of a monopole wrist-worn conformal bracelet antenna designed to operate at 850 MHz is shown in Fig. 20. This antenna is printed on a 0.035 mm thin, flexible Kapton substrate with $\epsilon_r = 3.8$ and is mounted on a 2 mm thick ABS plastic bracelet with $\epsilon_r = 2.8$ at 850 MHz. The monopole bracelet antenna [83] achieves a -10 dB impedance bandwidth of approximately 160 MHz, with a peak realized gain of -8.3 dBi and a radiation efficiency of 7% at 850 MHz. Additionally, for 23 dBm input power, the antenna in [83] exhibits a 10-g SAR value of 3.75 W/kg at $f_0 = 850$ MHz. This high SAR value was attributed to the small space (2 mm) between the antenna and the wrist.

Loop antennas have also been employed for Sub-GHz wristwatch applications [91], [92]. For instance, in [91], a

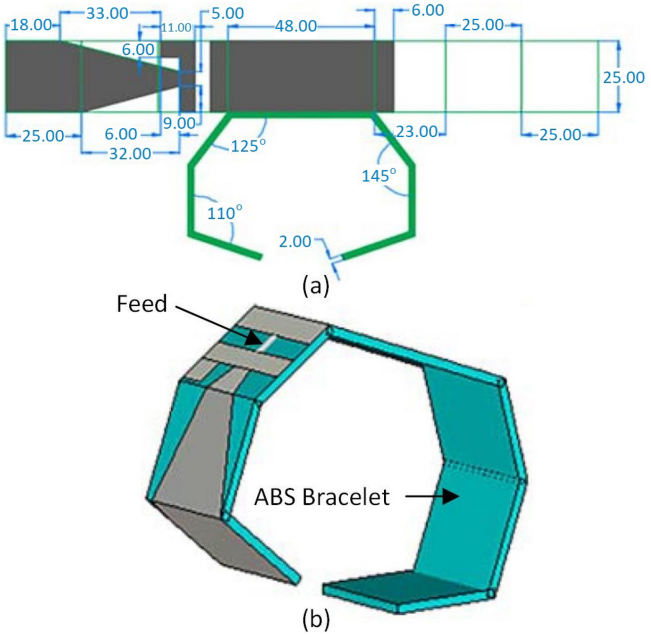

FIGURE 20. (a) Configuration of the monopole antenna on a flexible substrate, (b) Arrangement when the antenna is mounted on an ABS bracelet [83].

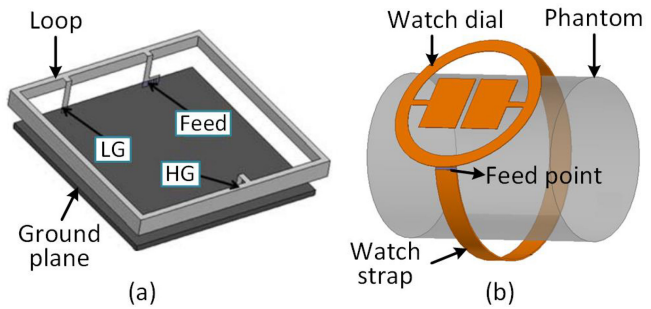

FIGURE 21. (a) Metal frame loop antenna [91], (b) Configuration of the wristwatch antenna reported in [92].

cellular metal frame loop antenna is reported and shown in Fig. 21(a). The antenna operates in two frequency bands (880–960 MHz and 1500–2200 MHz) with total dimensions of 40 mm × 30 mm × 10 mm. As depicted in Fig. 21(a), grounding points for the low band, denoted LG, and for the high band, denoted HG, are used to control the resonant frequencies of the antenna. The low band mode (880–960 MHz) has a half-wavelength resonant length measured from the feed point to LG through HG, as shown in Fig. 21(a). In the low band, the antenna exhibits a −10 dB impedance bandwidth of 180 MHz, but at the cost of a comparatively low radiation efficiency of less than 6% at f_0 = 920 MHz.

As shown in Fig. 21(b), a variant of a loop antenna using an annular ring, in conjunction with two rectangular patches for 915 MHz wristwatch applications is reported in [92]. The annular ring is internally loaded with two rectangular patches to lower the resonant frequency and to improve the impedance matching of the antenna. The antenna shown in

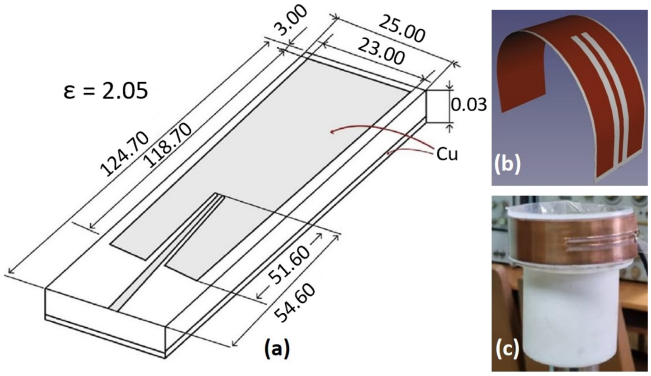

FIGURE 22. Geometry of the flexible antenna, the EM simulation model, and the fabricated prototype of the patch antenna [97].

Fig. 21(b) is made from a copper sheet and is placed 3 mm away from a simplified cylindrical human phantom model with a radius of 26 mm. This antenna achieves a −10 dB impedance bandwidth of approximately 100 MHz, with a peak realized gain of −8 dBi at the resonant frequency, f_0 = 915 MHz.

Microstrip patch antennas have also been used for Sub-GHz wristwatch antennas. For example, the development of a flexible wristband patch antenna for operation in the frequency range of 800–1300 MHz, suitable for applications in NB-IoT and LTE networks is presented in [97]. The geometry of the flexible antenna, the EM simulation model, and the fabricated prototype are shown in Fig. 22. The total size of this patch antenna is 124.5 mm x 25 mm and is designed and fabricated using a 50 μm metallic foil printed on a 30 μm thick polyethylene dielectric material. At 800 MHz, this antenna demonstrates a −10 dB impedance bandwidth of 28 MHz, a peak realized gain of −11.9 dBi, and a radiation efficiency of 38.6%.

A low profile flexible 915 MHz RFID-tag slotted patch antenna is presented in [98] and depicted in Fig. 23. The geometry of the proposed antenna is shown in Fig. 23(a-b) and Fig. 23(c) shows the arrangement when the antenna is attached to a human wrist. The bottom conductive surface (ground plane) of the PVC flexible substrate is metalized with adhesive copper tape that is shorted to the two rectangular copper areas on the left and right sides of the top of the PVC substrate. The copper structures on the top surface of the PVC substrate are then soldered to the left and right edges of the slotted patch, as shown in Fig. 23(b). Two T-shaped slots have been etched on a 0.4 mm FR-4 substrate that is placed on a 1.4 mm thick foam substrate. Varying the physical parameters (S_l, S_w and S_g) of the T-shaped slots affects the input impedance to provide conjugate impedance matching for the tag chip and adjust the resonant frequency of the antenna. This RFID tag antenna achieves a −10 dB impedance bandwidth of 19 MHz, which does not meet the required impedance bandwidth of 26 MHz for 915 band operation [116]. At f_0 = 915 MHz, this antenna achieves a peak realized gain of −6.87 dBi. This antenna is designed to

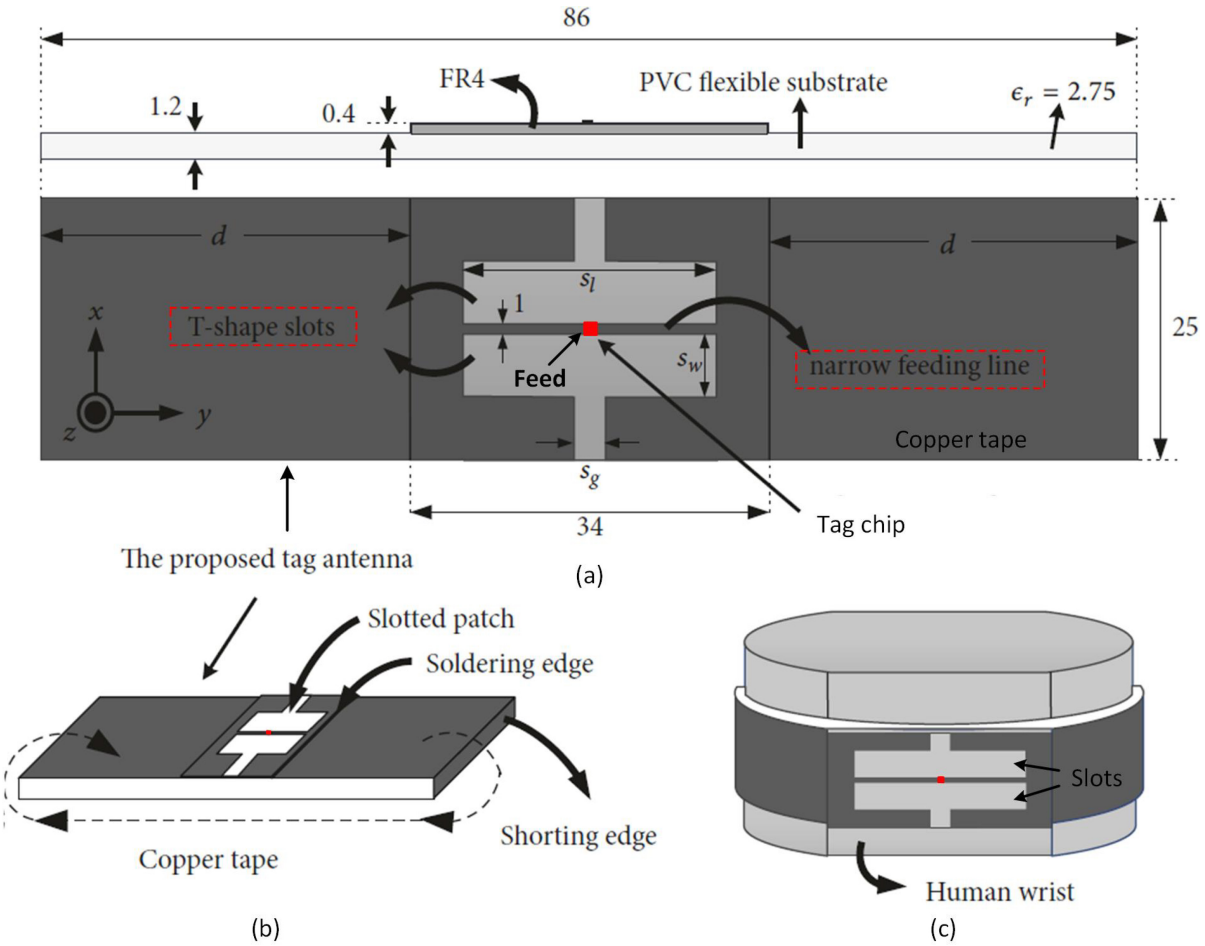

FIGURE 23. (a) Geometry of the proposed 915 MHz RFID tag antenna, d = 26, S_l = 24, S_W = 6, S_g = 3, Unit: mm, (b) Antenna attached to a human wrist [98].

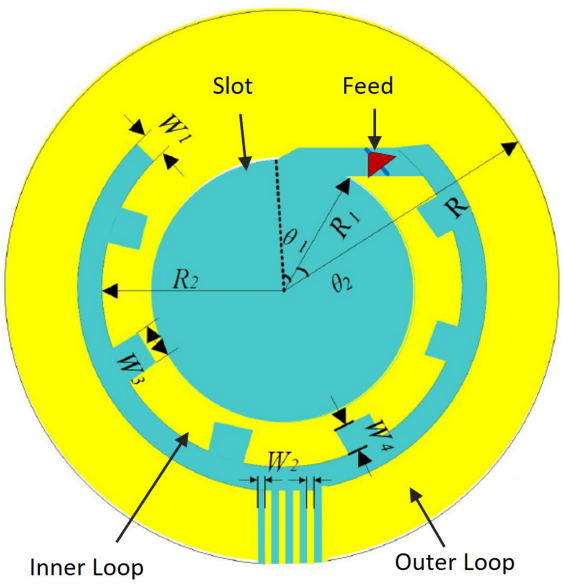

FIGURE 24. Geometry of the circular patch antenna reported in [96].

work when integrated into a wristband. However, due to its large dimensions (86 mm × 25 mm × 1.6 mm), this antenna is not ideal for integration into a practical-size wristwatch device where the antenna is not envisaged to be part of the strap.

In [96], the design of a compact dual-band circular patch antenna for smartwatch applications is reported. The geometry of the antenna is illustrated in Fig. 24. The antenna is designed using an FR4 substrate and has an overall dimension of $\pi \times 16^2 \times 0.52$ mm^3. This antenna covers both the LTE700/GSM850/GSM900 bands and the Bluetooth/Wi-Fi frequency bands. The design of this antenna is inspired by a split-ring resonator (SRR) structure, and it consists of an inner loop and an outer loop. The outer loop comprises distributed capacitive structures etched for impedance matching purposes. For this antenna, only the simulated results are reported, and when placed on a human wrist model, it exhibits a −10 dB impedance bandwidth of 195 MHz. Additionally, for a wrist-worn configuration, this antenna demonstrated a simulated peak realized gain of −11 dBi and a radiation efficiency of 8% at 850 MHz.

IV. PERFORMANCE ANALYSIS OF SUB-GHZ WRIST-WORN ANTENNAS

Table 2 summarizes the key performance characteristics of the 33 state-of-the-art Sub-GHz wrist-worn antennas that have been reviewed and discussed in detail in the previous

TABLE 2. On-phantom/on-body performance of state-of-the-art Sub-GHz wrist-worn antennas.

A	B	C	D	E	F	G	H	I
Row No.	Ref.	Antenna Topology	Dimensions $L \times W \times h$ (mm)	Resonant Frequency, f_0 (MHz)	-10 dB Bandwidth (MHz)	Gain at f_0 (dBi)	Efficiency at f_0 (%)	SAR at f_0 (W/kg)
1	[96]	Patch[1]	$\pi \times 16^2 \times 0.52$	850	195	-11	8	NA
2	[91]	Loop	$40 \times 30 \times 10$	920	180	NA	6.4	NA
3	[83]	Monopole	$127 \times 25 \times 2$	850	160	-8.3	7	3.75
4	[84]	Dipole	$145 \times 40 \times NA$	900	160	NA	6.3	0.18
5	[81]	IFA[2]	$93 \times 37 \times 5$	780	105[3]	NA	7.9	NA
6	[73]	PIFA[2]	$64.8 \times 45.6 \times 4.75$	866	105	-4.4	26	0.78
7	[92]	Loop	$201 \times 56 \times 0.2$	900	100	-8[1]	NA	NA
8	[88]	Monopole	$37 \times 43 \times 8$	930	95[3]	1.2[6]	30	0.54
9	[70]	PIFA	$48 \times 41 \times 2.3$	915	62	-4.6	17.8	0.0016
10	[39]	PIFA[2]	$44 \times 28 \times 1.6$	915	55[3]	-6.1	NA	NA
11	[85]	Dipole[2]	$220 \times 10 \times 0.25$	922.5	44	-11.2	NA	NA
12	[15]	PIFA	$48 \times 41 \times 2.3$	868	36[3]	-4.86	14.5	0.0027
13	[74]	PIFA[2]	$44 \times 44 \times 10$	767	35[3]	-5.4	14	NA
14	[75]	PIFA	$48 \times 41 \times 2.3$	915	30	-4.9	15.9	0.003
15	[76]	PIFA[1]	$188 \times 30 \times 6$	880	28	NA	83.7	NA
16	[97]	Patch	$124.7 \times 25 \times 0.03$	800	28	-11.9	38.6	NA
17	[112]	Dipole[1]	$117 \times 26 \times 0.277$	910	27	-11.87	45	NA
18	[77]	PIFA	$43.5 \times 28.5 \times 10.3$	915	26.4	-0.57	46.8	0.004
19	[93]	Helical	$40 \times 40 \times 14.4$	890	23	NA	NA	NA
20	[98]	Patch	$86 \times 25 \times 1.6$	915	19[5]	-6.87[1]	NA	NA
21	[94]	Helical	$110 \times 29 \times 1.55$	868	17	-13[1]	NA	NA
22	[89]	Monopole	$100 \times 15 \times 0.6$	911.25	14	-5.35	NA	NA
23	[87]	Dipole	$40 \times 20 \times 1.6$	915	9[5]	-3.2	14	NA
24	[90]	Monopole	$40 \times 15 \times 1.8$	911.25	7.5	-5.86	NA	NA
25	[82]	IFA[2]	$45 \times 30 \times 5.5$	846	7[1]	NA	14.8	NA
26	[86]	Dipole	$32 \times 25 \times 3.2$	925	6	-3.4	18	NA
27	[37]	PIFA[2]	$\pi \times 25^2 \times 5$	402.5	5.2[4,5]	-12	3.6	NA
28	[78]	PIFA	$\pi \times 25^2 \times 5$	402.5	4.22[4,5]	-9.2	6.9	NA
29	[38]	Loop[1]	$50 \times 35 \times 3$	868	3.5	-1.44	NA	0.0002
30	[95]	Spiral[1]	$\pi \times 16^2$	915	3[5]	-1.04	NA	NA
31	[79]	PIFA	$76.1 \times 13.6 \times 9.5$	866	NA	-6.6	8.6	NA
32	[99]	Patch[1]	$120 \times 29 \times 0.64$	867	NA	-13	NA	NA
33	[80]	PIFA	$90 \times 20 \times 3$	923	NA	-5	NA	NA

[1] Only simulated results are reported

[2] Antenna is fully integrated in a wristwatch device

[3] Antenna requires the use of an impedance matching network

[4] Only the -6 dB impedance bandwidth is reported

[5] Antenna does not meet the -10 dB bandwidth requirements for the targeted band

[6] Only free-space scenario is reported

Important Notes: (a) The above table is sorted in decreasing order of -10 dB bandwidth in column F, (b) NA = Information not reported.

section. Note that all the antennas listed in Table 2 were characterized using a phantom arm; however, the dielectric constant (ϵ_r) and electrical conductivity (σ) of the phantom arms used are different for different antennas. For instance, the phantom arm model used for the antenna in [39] has $\epsilon_r = 32.5$, $\sigma = 0.5$ S/m and the phantom arm used in [98] has $\epsilon_r = 41.3$, $\sigma = 0.87$ S/m at 915 MHz. For ease of reading, each reference is assigned a row number.

In Table 2, the columns denoted (A) to (I) respectively include, row number, publication reference, antenna topology, antenna dimensions (L = length, W = width, h = height in mm), f_0 = resonant frequency in MHz, BW = -10 dB impedance bandwidth in MHz, Gain = peak realized gain in dBi at f_0, η = radiation efficiency in % at f_0 and SAR = simulated specific absorption rate in W/kg at f_0. Note that Table 2 provides a list of the on-phantom/on-body

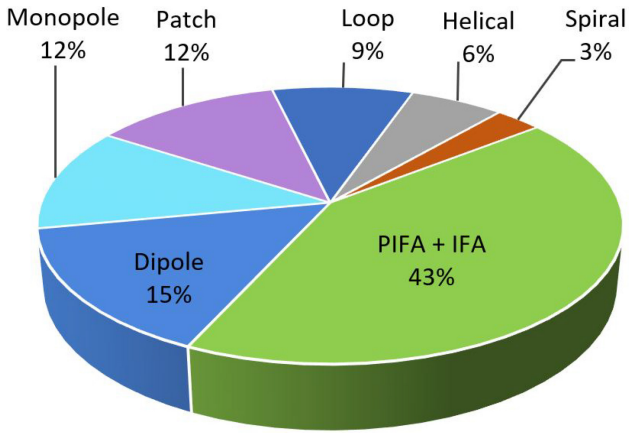

FIGURE 25. Topology distribution for Sub-GHz band wrist-worn antennas.

TABLE 3. −10 dB impedance requirements for popular Sub-GHz bands.

Frequency band (MHz)	Frequency range (MHz)	-10 dB Bandwidth (MHz)	Ref.
915	902 – 928	26	[116]
868	863 – 870	7	[121]
920	920 – 928	8	[116]
866	865 – 867	2	[122]
922.5	920 – 925	5	[123]
864	864 – 870	6	[122]
923	915 – 928	13	[122]
402.5	402 – 405	3	[78]
433	433.05 – 434.79	1.74	[122]

measured antenna parameters, unless otherwise specified in the table's footnote. In this section, Table 2 is studied in detail to analyze the key performance parameters of the state-of-the-art Sub-GHz wrist-worn antennas reported in the literature.

A. ANTENNA TOPOLOGY

As summarized in Column C of Table 2, various antenna topologies have been explored for Sub-GHz wristwatch applications, including patch antennas [96], [97], [98], [99], loop antennas [38], [91], [92], PIFA antennas [15], [37], [39], [70], [73], [74], [75], [76], [77], [78], [79], [80], IFA antennas [81], [82], dipole antennas [84], [85], [86], [87], [112], monopole antennas [83], [88], [89], [90], helical antennas [93], [94], and spiral antennas [95]. Among these, PIFA and IFA topologies are particularly favoured (see Fig. 25), comprising 43% of the antenna designs listed in Table 2. This preference is primarily attributed to their capability for integration into low-profile, compact-size wristwatch devices. Additionally, the finite ground plane of the PIFA and IFA serves as a shield against backward radiation towards the human wrist, helping to minimize losses that may occur due to interaction with human tissues [29], [37]. The PIFA topology is followed by the dipole and monopole antennas, accounting for 15% and 12% of the total distribution of Sub-GHz band wrist-worn antennas, respectively. The dipole and monopole topologies are particularly favoured in wristbands and smartwatches, where the radiating element of the antenna can be extended to the strap of these devices to take advantage of the additional antenna real estate provided by the strap [83], [84], [112].

It can be seen from Fig. 25 that other antenna topologies such as patch, loop, helical, and spiral antennas are notably less popular compared to PIFA, dipole, and monopole designs. This scarcity can be primarily attributed to the physical size constraints imposed by the compact form factor of modern smartwatches. At lower frequencies, such as those below 1 GHz, antennas based on patch, loop, helical, and spiral designs require significantly larger dimensions to achieve resonance effectively. For instance, designing a half-wavelength 868 MHz patch antenna using a standard FR4 substrate would theoretically require a minimum length of approximately 82 mm [117], making it impractical for integration into a typical smartwatch such as an Apple Watch Series 9 with dimensions of 45 mm × 41 mm × 10.7 mm. To address these challenges, researchers have employed various miniaturization techniques to reduce the size of antennas. However, these techniques often come at the expense of compromised antenna performance. For example, miniaturized patch antennas [96], [97], [99], loops [91], [92], and helical antenna [94] have exhibited degraded radiation characteristics. Similarly, miniaturized loop [38] and spiral [95] antennas have demonstrated narrower bandwidths compared to their larger counterparts.

B. −10 DB IMPEDANCE BANDWIDTH

One of the main challenges in designing antennas for Sub-GHz bands for integration into wrist-worn devices of practical size is the limited impedance bandwidth associated with electrically small antennas [70], [118]. The antennas listed in Table 2 are sorted in decreasing order of −10 dB impedance bandwidth, as indicated in column F. The −10 dB impedance requirements of the various Sub-GHz bands have been summarized in Table 3. It is observed from Table 2 that the five antennas in rows 1 to 5 [81], [83], [84], [91], [96] achieve the largest −10 dB impedance bandwidth performance in the list. It can be highlighted that there exists a fundamental trade-off limit between impedance bandwidth and radiation efficiency of electrically small antennas [119], and these five antennas achieve a wider impedance bandwidth of ≥ 105 MHz but at the expense of a lower radiation efficiency of ≤8%. The PIFA antenna in row 6 [73] has a −10 dB impedance bandwidth of 105 MHz. However, this antenna uses a wrist strap that has a width of 50 mm, which is considerably wider than a standard wristwatch strap, such as those found on an Apple smartwatch which is 24 mm wide [14]. The antennas in rows 5, 8, 10, 12, and 13 achieve a −10 dB impedance bandwidth of 105 MHz, 95 MHz, 55 MHz, 36 MHz and 35 MHz, respectively. However,

through the use of impedance-matching networks for bandwidth enhancement. While effective, this solution introduces additional RF losses, increases costs, and complicates the design process [120]. All of the antennas in rows 11, 16, and 17 respectively achieve a −10 dB bandwidth of more than 27 MHz, meeting the impedance bandwidth required for the targeted band. However, all three of these antennas have a comparatively low peak realized gain of less than −11 dBi at their respective resonant frequencies. All three PIFA antennas listed in rows 9, 14, and 18 employ a dual-radiator approach to enhance the impedance bandwidth of the antenna and demonstrate a −10 dB impedance bandwidth exceeding the required 26 MHz bandwidth for 915 MHz band operations. The PIFA antenna in row 15 achieves a −10 dB impedance bandwidth of 28 MHz, but this antenna occupies a size of 188 mm × 30 mm × 6 mm, which is too large for practical integration into devices akin to an Apple smartwatch [14].

The analysis of Sub-GHz wrist-worn antennas, as highlighted in Table 2, points to a prevalent challenge: a significant number of these antennas struggle to achieve a satisfactory −10 dB impedance bandwidth, particularly for the demands of specific frequency bands. Notably, antennas designed for the 915 MHz band, such as those detailed in rows 20, 23, and 30 of the referenced table, exhibit −10 dB impedance bandwidths of 19 MHz, 9 MHz, and 3 MHz respectively. These values fall short of the minimum 26 MHz bandwidth requirement for the 915 MHz ISM band, a standard defined by the IEEE 802.15.4 standard for operation within this spectrum [116]. Furthermore, antennas tailored for the Medical Implant Communication Service (MICS) band, specifically mentioned in rows 27 and 28, only achieve a −6 dB impedance bandwidth. These MICS band antennas do not satisfy the minimum required −10 dB impedance bandwidth of 3 MHz for MICS band operation (402 – 405 MHz) [78]. Based on the impedance bandwidth analysis of the 33 published works listed in Table 2, a gap in the state-of-the-art concerning the limited impedance bandwidth is evident. It is observed that the majority of wristwatch antennas exhibit a restricted −10 dB impedance bandwidth of less than 20 MHz (rows 20 to 30), or achieve a wider impedance bandwidth exceeding 20 MHz by either designing the antenna impractically large for a wristwatch device (rows 5-7, 15, 19) or at the expense of impaired radiation performance (rows 1, 3, 11, 16, 17, 21, 27, 28, 32). Consequently, there is a clear need for the development of new compact antenna designs capable of achieving enhanced impedance bandwidth while simultaneously maximizing radiation performance.

C. PEAK REALIZED GAIN AT F_0

Having studied the −10 dB impedance bandwidth performance of a total of 33 Sub-GHz wristwatch antennas, the *On-phantom/on-body* peak realized gain performance, as summarized in Column G of Table 2 is now analyzed. The 915 MHz PIFA antenna in row 18 exhibits the highest on-phantom peak realized gain of −0.57 dBi. The spiral antenna in row 30 shows the second-highest peak realized gain of −1.04 dBi at 915 MHz. this antenna has a −10 dB impedance bandwidth of only 3 MHz and does not meet the minimum 26 MHz requirement for 915 MHz band operation. Similarly, the 868 MHz loop antenna in row 29 demonstrates the third-highest peak realized gain of −1.44 dBi, but it only achieves a −10 dB impedance bandwidth of 3.5 MHz. The 868 MHz helical antenna in row 21 exhibits the lowest gain performance among the 33 antennas reviewed, with a peak realized gain of −13 dBi at 868 MHz. As evident from Table 2, the peak realized gain of wrist-worn Sub-GHz antennas exhibits significant variation, ranging from −13 dBi for electrically small antennas in [94], [99] to −0.57 dBi for a PIFA antenna [77], when worn on the human body. This disparity in gain can be attributed to several key factors:

- *Antenna physical size and ground plane dimensions:* Smaller antennas, such as those in [94], [99], typically exhibit lower gain due to their reduced radiation resistance and increased losses. Larger ground planes can enhance gain by improving the antenna's directivity and reducing backlobe radiation.
- *Proximity of the radiator to the human body:* Antennas positioned very close (e.g., less than 0.3 mm) to the lossy human tissue, such as those in [97], [112], suffer from increased absorption losses, resulting in lower radiation efficiency and gain.
- *Substrate and enclosure material properties:* The dissipation factor of the substrate and enclosure materials can impact antenna efficiency and, consequently, gain. Low-loss materials are preferred for optimal performance [117].
- *Presence of internal smartwatch components:* Many antennas, such as those in [15], [37], [39], [70], [73], [75], [81], [82], [91] are integrated into practical wristwatch devices. The close proximity of internal components to the radiating element can introduce losses and influence the antenna's gain performance.
- *Inherent characteristics of antenna topologies:* Different antenna topologies exhibit varying gain performance due to their inherent radiation mechanisms and field distributions [117].

Furthermore, a fundamental trade-off exists between gain and impedance bandwidth in antenna design. Some antennas, such as those in [83], [96], sacrifice gain to achieve wider impedance bandwidths, while others, like the spiral antenna in [95], prioritize gain at the expense of bandwidth. These factors, along with the complex electromagnetic interactions between the antenna, the smartwatch, and the human body, underscore the challenges in designing high-performance wrist-worn Sub-GHz antennas. Antenna designers must carefully consider and balance these factors to optimize antenna gain and radiation efficiency for real-world usage scenarios.

It is also noteworthy that out of the 33 antennas reviewed in Table 2, only 10 antennas as listed in rows 6, 9, 12, 14, 18, 23, 26, 29, 30, and 33, achieve a peak realized gain ≥ -5 dBi. Note that a peak realized gain of -5 dBi does not represent a defined threshold value. However, a close analysis of the antenna parameters summarized in Table 2 reveals a pattern that when the gain of the antenna is close to -5 dBi, the antenna simultaneously achieves good impedance bandwidth ($\geq$26 MHz required for the 915 MHz band) and radiation efficiency (close to or greater than 15%) as in [15], [39], [70], [73], [74], [75]. Furthermore, 6 antennas, listed in rows 2, 4, 5, 15, 19, and 25 of Table 2 do not report the peak realized gain figures.

D. RADIATION EFFICIENCY AT F_0

After analyzing the -10 dB impedance bandwidth and peak realized gain requirements, in this section the radiation efficiency performance, as listed in Column H of Table 2, is next investigated. It is observed that more than 36% (12 out of 33) of the Sub-GHz wristwatch antennas do not report radiation efficiency performance figures, either measured or simulated. The PIFA antenna in row 15 achieves the highest radiation efficiency of 83.7% for all 33 antennas but this antenna occupies a considerable size of 188 mm $\times$ 30 mm $\times$ 6 mm, which is not suitable for integration into a practical wristwatch device [14]. The majority (total 12 antennas) of Sub-GHz antennas (rows 1-5, 12, 13, 23, 25, 27, 28, 31) have a radiation efficiency of less than 15%, and only 9 antennas (rows 6, 8, 9, 14-18, 26) out of 33 antennas analyzed achieve a radiation efficiency of greater than 15%.

E. SPECIFIC ABSORPTION RATE (SAR) F_0

Table 2 column (I) summarizes the SAR performance figures for the 33 antennas analyzed. The SAR parameter is a measure of the rate at which RF power is absorbed by the human body when exposed to EM radiation [113] and for wrist-worn wireless devices, the SAR level should not exceed a limit of 4.0 W/kg averaged over 10-g of wrist tissue [107], [115]. Therefore, the SAR figure is an important parameter to consider when designing a wristwatch antenna. However, it is observed that the majority of Sub-GHz wrist-worn antennas described in the literature do not report SAR performance. Out of the 33 antennas reviewed, SAR performance is reported for only 9 antennas (rows 3, 4, 6, 8, 9, 12, 14, 18, 29), which accounts for only 27% of all the antennas listed in Table 2.

F. WRISTWATCH MODEL

This analysis of the literature also has found that the majority of Sub-GHz wristwatch antennas, with the exception of antennas in rows 2, 5, 6, 9, 10, 12-14, 25, and 27 do not consider the potential performance degradation due to internal wristwatch components in close proximity to the antenna, something that is inevitable in a practical wristwatch device. The internal components of a practical wristwatch device typically include printed circuit boards (PCBs), battery, sensor assemblies, connectors and metal screws for example. These internal components can significantly impact the performance of the integrated antenna, primarily by causing impedance mismatches and reducing radiation efficiency. Metallic components, such as PCBs and battery casings are particularly problematic when positioned near the antenna's radiating element. These components can reflect and reradiate electromagnetic waves, leading to signal distortion and ohmic losses. Hence, precise placement and orientation of the antenna within the wristwatch case are crucial to minimize interference with other internal components [124]. Furthermore, positioning the radiating element furthest from the human body along with optimizing the shape and size of the ground plane can help to reduce energy absorption by the human body. Overall, meticulous consideration of antenna placement, design, tuning, and shielding techniques is imperative to mitigate the effects of internal components and optimize antenna performance in smartwatches.

Drawing from the detailed literature review discussed above, Table 4 outlines the gaps in the existing literature by summarizing the key challenges, limitations, and issues related to antenna size, impedance bandwidth, peak realized gain, radiation efficiency, SAR and wristwatch integration challenges with Sub-GHz wrist-worn antennas. A critical observation is that 15% of the antennas fail to meet the impedance bandwidth requirements for their targeted bands, which can significantly impact their performance in real-world applications. Another notable finding is the lack of comprehensive reporting on key antenna parameters, with 18% of the papers not providing data on antenna gain, 36% omitting radiation efficiency, and a staggering 73% lacking information on SAR figures. Moreover, only 30% of the reviewed antennas are integrated into physical wristwatch devices, highlighting a gap between theoretical designs and practical implementations. This limited integration into real-world devices hinders the understanding of antenna performance in the presence of various smartwatch components and user interaction. Perhaps most concerning is that only 21% of the reviewed papers consider all the critical antenna parameters, such as impedance bandwidth, gain, radiation efficiency, and SAR. This deficiency in comprehensive reporting impedes a thorough understanding of the antennas' performance characteristics and their suitability for practical applications.

V. FUTURE PERSPECTIVES

The global market for wrist-wear wireless sensing technology is experiencing ongoing proliferation and diversification [8], [10]. The future perspective of designing innovative antennas for these wrist-worn wireless sensing devices holds great promise for enhancing connectivity and seamless integration into our daily lives. Therefore, it will be worth exploring various emerging innovative materials, methods, and techniques for designing next-generation

TABLE 4. Challenges and limitations with state-of-the-art Sub-GHz wrist-worn antennas in the literature (33 papers summarized in Table 2).

No.	Challenging parameters	References
1	5 out of 33 antennas (i.e., 15%) fail to meet the -10 dB impedance bandwidth (BW) requirements for the targeted band	[37], [78], [87], [95], [98]
2	3 out of 33 papers (9%) do not report impedance bandwidth or S_{11} response	[79], [80], [99]
3	11 out of 33 antennas have an impedance bandwidth of less than 20 MHz	[37], [38], [78], [87], [95], [98] [82], [86], [89], [90], [94]
4	Only 10 out of 33 papers (30%) achieve a peak realized gain of -5 dBi or higher	[15], [70], [73], [75], [77] [38], [80], [86], [87], [95]
5	6 out of 33 papers (18%) do not provide information on antenna gain	[76], [81], [82], [84], [91], [93]
6	Only 9 out of 33 antennas (27%) exhibit a radiation efficiency of 15% or higher	[70], [73], [75], [76], [88] [77], [86], [97], [112]
7	12 of the 33 papers (more than 36%) do not report radiation efficiency	[39], [85], [92]–[94], [98] [38], [80], [89], [90], [95], [99]
8	Only 9 out of 33 papers report specific absorption rate (SAR) figures	[70], [73], [83], [84], [88] [15], [38], [75], [77]
9	Only 7 out of 33 papers (21%) report all the key antenna parameters such as bandwidth, gain, efficiency, and SAR	[70], [73], [83], [88] [15], [75], [77]
10	Only 10 out of the 33 antennas consider the physical wristwatch device and its internal components	[39], [70], [73], [81], [91] [15], [37], [74], [75], [82]

wrist-worn antennas. As advancements in miniaturization techniques and material science continue, increasingly compact and efficient antennas can be anticipated to be integrated into smartwatches, enabling a broader range of communication protocols. Next-generation smartwatch-based wireless sensing devices are expected to incorporate enhanced physical layer security, radio frequency (RF) wireless charging, faster data transfer rates, and low latency. Additionally, there is anticipation for increased utilization of emerging artificial intelligence (AI) methods in antenna design optimization. This is coupled with a rise in the adoption of additive manufacturing technologies (e.g., 3D printing, screen printing, and inkjet printing), as well as the use of transparent conductive materials for antenna fabrication.

The smartwatch antenna in [125] demonstrated enhanced physical layer security through directional modulation using beam-steerable wrist-worn antennas. Furthermore, the antenna described in [126] utilizes the theory of spherical modes to design a 3D beam-steering MIMO antenna to enhance the physical layer security. While the antennas in [125], [126] are tailored for Sub-6 GHz frequencies (5.57 GHz and 5.75 GHz), the implementation of a similar beam-steerable design concept holds the potential for enhancing physical layer security in Sub-GHz wrist-worn antennas, facilitating secure communication over LoRaWAN, NB-IoT, and Sigfox wireless technologies. Additionally, enabling the Internet of Everything (IoE) everywhere using future LoRaWAN over satellite for wearable devices in remote areas has the potential to enhance the functionality of IoT connectivity on a global scale [127], [128].

In the realm of wearable technology, the future of wrist-worn antennas appears promising with continuous advancements in miniaturization techniques [129], [130] and integration with additive manufacturing technologies [131], [132], [133], such as 3D printing [134], screen printing [135], [136], and inkjet printing [137], [138]. Antenna miniaturization facilitates sleeker and more aesthetically pleasing designs, thereby enhancing user comfort and wearability [139]. The authors of [129], [130] discuss several antenna miniaturization techniques, such as implementing space-filling curves, fractal geometries, meander lines, engineered ground planes, reactive loading, high-dielectric constant substrates, 3D printing for complex geometries, slow-wave structures, and metamaterials. One or a hybrid of more than one antenna miniaturization technique can be utilized to design compact, highly integrated antennas for smartwatch wireless sensing devices. Additionally, compact antennas can be designed using screen printing and inkjet printing techniques. With these printing methods, conductive ink can be directly applied onto the smartwatch enclosure or its internal components to create the desired antenna pattern. Furthermore, the optimization of next-generation antennas is expected to be driven by emerging artificial intelligence (AI)-based modeling techniques aimed at achieving antenna miniaturization and enhancing antenna performance across various applications, including smartwatches [140]. For example, in [141], [142], machine learning (ML) and deep learning (DL) regression modeling techniques have been employed for antenna miniaturization. A miniaturized chipless RFID sensor tag antenna design, as described in [141], is achieved by utilizing a feedforward artificial

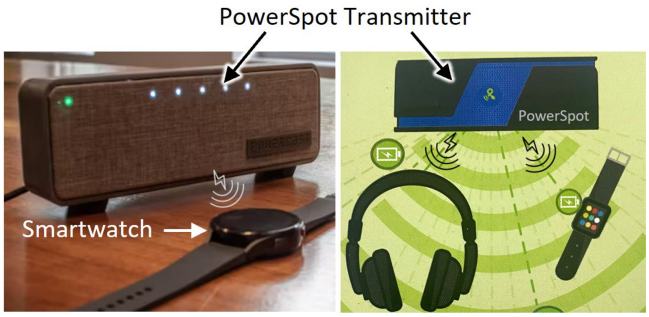

FIGURE 26. Far-field RF wireless charging system for smartwatches [144], [145].

neural network (ANN) to optimize the solution with all possible design combinations.

The integration of wireless power charging and energy harvesting mechanisms is poised to revolutionize the autonomy of these devices. The integration of wireless charging not only eliminates the inconvenience of cables but also contributes to environmental sustainability by reducing electronic waste associated with traditional charging methods [138], [143]. In recent years, the concept of far-field RF wireless charging, as opposed to the currently ubiquitous wired and Qi-enabled charging has gained notable popularity. In this context, a smartwatch-integrated antenna plays a crucial role in receiving the RF power transmitted by a charging transmitter. For instance, Powercast has recently introduced an RF wireless charging concept for smartwatches operating at the 915 MHz band. As depicted in Fig. 26, the RF wireless charging system comprises a transmitter (e.g., PowerSpot) that emits RF energy, and a receiver embedded within PowerSpot-enabled electronic devices (e.g., smartwatches, headphones, etc.) captures this energy and converts it into electrical power to charge the device's battery [144]. This technology can enable the wireless charging of a smartwatch from a distance of as far as 20 meters [145]. Therefore, the design of innovative, compact, high-gain, and efficient antennas holds paramount importance for the advancement of RF wireless charging solutions tailored for smartwatches.

The use of transparent antennas in future wearable smartwatches can play a pivotal role in providing users with a seamless and visually aesthetic technological experience. As the demand for stylish designs in wearable technology grows, transparent antennas offer an innovative solution by integrating seamlessly into the device without compromising its visual appeal [146]. These antennas, made from transparent conductive materials [147], enable desired efficient signal transmission while remaining discreetly embedded within the watch's display or casing [148]. The use of transparent materials to design optically transparent antennas for smartwatches can closely be correlated with optically transparent antennas reported in the literature for smart glasses [149] and smartphones [150]. However, it is important to emphasize that utilizing transparent materials for antenna design is expected to lead to a degradation in antenna performance, primarily due to their inherently lower conductivity, resulting in increased ohmic losses and decreased efficiency. Therefore, finding conductive materials with an optimal balance of conductivity and optical transparency presents a significant challenge [146].

Metamaterials are artificially engineered materials with unique electromagnetic properties not commonly found in nature. In antenna design, metamaterials are utilized to enhance performance parameters such as impedance bandwidth, gain, and miniaturization, while also mitigating the absorption of radiated power by the human body in wearable applications [151]. High impedance surfaces (HIS), a type of metamaterial structure, have been employed at 2.4 GHz to improve the performance of wristwatch antennas, as discussed in [152], [153], [154]. HIS structures facilitate performance enhancement (e.g., antenna gain) by ensuring that the image current in the HIS flows in-phase and parallel to the original current distribution in the radiating element, thereby minimizing the power radiated towards the lossy human body [152], [154]. However, integrating HIS into antennas operating at sub-GHz frequencies would necessitate designing HIS structures of electrically large size, posing challenges for their realization in compact wristwatch devices. Research and investigation into incorporating metamaterials (e.g., HIS) at sub-GHz frequencies would be promising for improving the performance of next-generation sub-GHz wrist-worn antennas.

Due to the wearer's movements and activities, maintaining a consistent orientation for smartwatch antennas in relation to external receivers such as LoRa gateways or RFID readers becomes practically impossible. To address these challenges and ensure robust data communication, the adoption of circularly polarized (CP) antennas emerges as an optimal solution. CP antennas exhibit greater immunity to interferences and multipath fading, while also offering flexible orientation for the smartwatch antennas [155]. In [26], a metal-bezel smartwatch with a 1.57 GHz antenna for the Global Positioning System (GPS) achieves CP characteristics with the aid of a lumped capacitor positioned between the metal radiating ring and the ground plane. Utilizing a metal plane, this antenna also features a method to mitigate the impact of the human wrist on antenna performance. Similarly, in [16], for the GPS antenna, circular polarization is achieved through the use of two lumped capacitors connected between the system ground and the radiating metal ring. In [156] reactive loads are employed at proper locations of the metallic frame of the 1.575 GHz smartwatch antenna to achieve the CP performance. Furthermore, for a 27.5 GHz 5G-enabled substrate integrated waveguide (SIW) antenna in [157] CP characteristics have been achieved by employing a modified circular-shaped split-ring slot and four strategically placed metallic shorting vias. Although achieving circularly polarized characteristics at Sub-GHz frequencies will pose a significant challenge due to the confined space within practical smartwatches, exploring new design methods to incorporate CP into future Sub-GHz smartwatch antennas would be worthwhile.

VI. CONCLUSION

For the first time, this paper presented a detailed review of state-of-the-art Sub-GHz wrist-worn antennas for wireless sensing applications. The paper first showed that there is an emerging market for the use of smartwatch devices, particularly in commercial wireless health monitoring, fitness, and activity tracking applications. The paper also showed the potential of Sub-GHz technologies (e.g., LoRaWAN, NB-IoT, and Sigfox) to offer long-range wireless communication with low power consumption for these types of wrist-worn applications. Modern wrist-worn devices are highly integrated and require the design of compact and efficient antenna structures that necessitate the use of electrically small antennas. This paper comprehensively reviewed Sub-GHz wrist-worn antennas, focusing on analyzing key antenna performance parameters and paving the way for a better understanding of the design challenges, limitations, and future trends for antenna design. Among the large number of antenna topologies reviewed, the planar inverted-F antenna (PIFA) emerged as one of the most popular solutions for use in wristwatch devices due to its compact and low-profile characteristics, as well as its ability to minimize backward radiation toward the human wrist tissue. This study also showed that achieving the required impedance bandwidth for the targeted frequency band, while maintaining the desired antenna efficiency and gain is one of the key challenges in designing antennas for practical wrist-worn devices. Additionally, the paper presented future perspectives for realizing Sub-GHz wrist-worn antennas using a variety of methods and techniques, including additive manufacturing, enhanced physical layer security, LoRaWAN for satellite communication, machine learning optimization, RF wireless charging, adoption of metamaterials, and the utilization of transparent materials to develop innovative antennas for next-generation wrist-worn wireless sensing solutions.

REFERENCES

[1] P. Sundaravadivel, E. Kougianos, S. P. Mohanty, and M. K. Ganapathiraju, "Everything you wanted to know about smart health care: Evaluating the different technologies and components of the Internet of Things for better health," *IEEE Consum. Electron. Mag.*, vol. 7, no. 1, pp. 18–28, Jan. 2018.

[2] J. W. Kim, J. H. Lim, S. M. Moon, and B. Jang, "Collecting health lifelog data from smartwatch users in a privacy-preserving manner," *IEEE Trans. Consum. Electron.*, vol. 65, no. 3, pp. 369–378, Aug. 2019.

[3] G.-Z. Yang, *Body Sensor Networks*, 2nd ed. London, U.K.: Springer, 2014.

[4] E. G. Zimbelman and R. F. Keefe, "Development and validation of smartwatch-based activity recognition models for rigging crew workers on cable logging operations," *PLoS ONE*, vol. 16, no. 5, pp. 1–25, May 2021. [Online]. Available: https://doi.org/10.1371/journal.pone.0250624

[5] J. S. Park, S. Robinovitch, and W. S. Kim, "A wireless wristband accelerometer for monitoring of rubber band exercises," *IEEE Sensors J.*, vol. 16, no. 5, pp. 1143–1150, Mar. 2016.

[6] T. M. Fernández-Caramés and P. Fraga-Lamas, "Towards the Internet of smart clothing: A review on IoT wearables and garments for creating intelligent connected e-textiles," *Electronics*, vol. 7, no. 12, p. 405, 2018. [Online]. Available: https://www.mdpi.com/2079-9292/7/12/405

[7] W.-J. Chang, L.-B. Chen, and Y.-Z. Chiou, "Design and implementation of a drowsiness-fatigue-detection system based on wearable smart glasses to increase road safety," *IEEE Trans. Consum. Electron.*, vol. 64, no. 4, pp. 461–469, Nov. 2018.

[8] M. M. Hosseini, S. T. M. Hosseini, K. Qayumi, S. Hosseinzadeh, and S. S. S. Tabar, "Smartwatches in healthcare medicine: Assistance and monitoring: A scoping review," *BMC Med. Informat. Decis. Making*, vol. 23, no. 1, p. 248, 2023.

[9] D. S. Bhatti et al., "A survey on wireless wearable body area networks: A perspective of technology and economy," *Sensors*, vol. 22, no. 20, p. 7722, 2022.

[10] "Market.us: Global wearable technology market by product." Accessed: Jan. 24, 2024. [Online]. Available: https://market.us/report/wearable-technology-market/

[11] A. Mishra and R. J. Stanislaus, "Smart watch supported system for health care monitoring," 2023, *arXiv:2304.07789*.

[12] M. E. E. Alahi, N. Pereira-Ishak, S. C. Mukhopadhyay, and L. Burkitt, "An Internet-of-Things enabled smart sensing system for nitrate monitoring," *IEEE Internet Things J.*, vol. 5, no. 6, pp. 4409–4417, Dec. 2018.

[13] "GII global information: Wearable technology market by device, by product type, by application: Global opportunity analysis and industry forecast, 2020–2031." Accessed: Jan. 24, 2024. [Online]. Available: https://www.giiresearch.com/report/amr1090907-wearable-technology-market-by-device-by-product.html

[14] "Apple watch series 9." Accessed: Feb. 10, 2024. [Online]. Available: https://www.apple.com/ie/shop/buy-watch/apple-watch

[15] S. Kumar et al., "A wristwatch-based wireless sensor platform for IoT health monitoring applications," *Sensors*, vol. 20, no. 6, p. 1675, 2020. [Online]. Available: https://www.mdpi.com/1424-8220/20/6/1675

[16] Z. Xu and Y. Wang, "Design of triple-band antenna for metal-bezel smartwatches with circular polarization in both GPS L5/L1 bands," *IEEE Trans. Antennas Propag.*, vol. 72, no. 3, pp. 2926–2931, Mar. 2024.

[17] T. Lu, C. Fu, M. Ma, C. Fang, and A. Turner, "Healthcare applications of smart watches. A systematic review," *Appl. Clin. Inform.*, vol. 7, no. 3, pp. 850–869, 2016.

[18] H. Yu, S. Cang, and Y. Wang, "A review of sensor selection, sensor devices and sensor deployment for wearable sensor-based human activity recognition systems," in *Proc. 10th Int. Conf. Softw. Knowl. Inf. Manag. Appl. (SKIMA)*, 2016, pp. 250–257.

[19] "Huawei watch GT 2 Pro." Accessed: Feb. 10, 2024. [Online]. Available: https://consumer.huawei.com/ie/wearables/watch-gt2-pro/

[20] "Garmin vivoactive 4." Accessed: Feb. 10, 2024. [Online]. Available: https://buy.garmin.com/en-IE/GB/p/643382

[21] "Fitbit sense." Accessed: Feb. 10, 2024. [Online]. Available: https://www.fitbit.com/global/ie/products/smartwatches/sense

[22] "Samsung galaxy watch active." Accessed: Feb. 10, 2024. [Online]. Available: https://www.samsung.com/in/microsite/galaxy-watch-active/

[23] "Fossil Gen 5." Accessed: Feb. 10, 2024. [Online]. Available: https://www.fossil.com/en-us/smartwatches/learn-more/gen-5/

[24] K. N. Paracha, S. K. A. Rahim, P. J. Soh, and M. Khalily, "Wearable antennas: A review of materials, structures, and innovative features for autonomous communication and sensing," *IEEE Access*, vol. 7, pp. 56694–56712, 2019.

[25] R. M. Al-Eidan, H. Al-Khalifa, and A. M. Al-Salman, "A review of wrist-worn wearable: Sensors, models, and challenges," *J. Sensors*, vol. 2018, pp. 1–20, 2018.

[26] Z. Xu and Y. Wang, "Design of dual-band antenna for metal-bezel smartwatches with circular polarization in GPS band and low wrist effect," *IEEE Trans. Antennas Propag.*, vol. 71, no. 6, pp. 4651–4662, Jun. 2023.

[27] R. F. Harrington, "Effect of antenna size on gain, bandwidth, and efficiency," *J. Res. Nat. Bureau Stand.*, vol. 64, no. 1, pp. 1–12, 1960.

[28] S. Kumar, R. B. V. B. Simorangkir, D. R. Gawade, A. J. Quinn, B. O'Flynn, and J. L. Buckley, "An 868 MHz bandage type antenna using aluminum conductor and PDMs substrate," in *Proc. Int. Workshop Antenna Technol. (iWAT)*, 2022, pp. 90–92.

[29] V. F. Fusco, *Foundations of Antenna Theory and Techniques*. London, U.K.: Pearson, 2005.

[30] Y. Huang, Z. Chen, D. Liu, H. Nakano, X. Qing, and T. Zwick, "Radiation efficiency measurements of small antennas," in *Handbook of Antenna Technologies*, vol. 3. Singapore: Springer, 2016, pp. 2165–2189.

[31] M. I. Hossain, M. I. Faruque, and M. T. Islam, "Investigation of hand impact on PIFA performances and SAR in human head," *J. Appl. Res. Technol.*, vol. 13, no. 4, pp. 447–453, 2015. [Online]. Available: https://www.sciencedirect.com/science/article/pii/S1665642315000449

[32] A. Alomainy, Y. Hao, and D. M. Davenport, "Parametric study of wearable antennas with varying distances from the body and different on-body positions," in *Proc. IET Seminar Antennas Propag. Body-Centric Wireless Commun.*, 2007, pp. 84–89.

[33] A. J. Khalilabadi and A. Zadehgol, "An ultra-thin dual-band smart-watch antenna compatible with several wireless bands," in *Proc. IEEE Int. Symp. Antennas Propag. USNC/URSI Nat. Radio Sci. Meeting*, 2018, pp. 457–458.

[34] S. Y. Jun, A. Elibiary, B. Sanz-Izquierdo, L. Winchester, D. Bird, and A. McCleland, "3-D printing of conformal antennas for diversity wrist worn applications," *IEEE Trans. Compon. Packag. Manuf. Technol.*, vol. 8, no. 12, pp. 2227–2235, Dec. 2018.

[35] Y. Jin and J. Choi, "Bandwidth enhanced compact dual-band smart watch antenna for WLAN 2.4/5.2 GHz application," in *Proc. Int. Appl. Comput. Electromagn. Soc. Symp. (ACES)*, 2017, pp. 1–2.

[36] S. Woo, J. Baek, H. Park, D. Kim, and J. Choi, "Design of a compact UWB diversity antenna for WBAN wrist-watch applications," in *Proc. Int. Symp. Antennas Propag.*, vol. 2, 2013, pp. 1304–1306.

[37] H. Hamouda, P. L. Thuc, R. Staraj, and G. Kossiavas, "Small antenna embedded in a wrist-watch for application in telemedicine," in *Proc. 8th Eur. Conf. Antennas Propag. (EuCAP)*, 2014, pp. 876–879.

[38] M. Feliziani and F. Maradei, "Antenna design of a UHF RFID tag for human tracking avoiding spurious emission," in *Proc. IEEE Int. Symp. Electromagn. Compatib.*, 2012, pp. 245–248.

[39] A. Di Serio et al., "Potential of sub-GHz wireless for future IoT wearables and design of compact 915 MHz antenna," *Sensors*, vol. 18, no. 1, pp. 1–22, 2018. [Online]. Available: https://www.mdpi.com/1424-8220/18/1/22

[40] "LoRa Alliance." Accessed: Feb. 10, 2024. [Online]. Available: https://lora-alliance.org/

[41] "NB-IoT frequency bands." Accessed: Feb. 6, 2024. [Online]. Available: https://portal.3gpp.org/desktopmodules/Specifications/SpecificationDetails.aspx?specificationId=2965

[42] "Sigfox frequency bands." Accessed: Feb. 6, 2024. [Online]. Available: https://build.sigfox.com/sigfox-radio-configurations-rc

[43] F. Wu, C. Qiu, T. Wu, and M. R. Yuce, "Edge-based hybrid system implementation for long-range safety and healthcare IoT applications," *IEEE Internet Things J.*, vol. 8, no. 12, pp. 9970–9980, Jun. 2021.

[44] S. Popli, R. K. Jha, and S. Jain, "A survey on energy efficient narrowband Internet of Things (NBIoT): Architecture, application and challenges," *IEEE Access*, vol. 7, pp. 16739–16776, 2019.

[45] E. De Poorter et al., "Sub-GHz LPWAN network coexistence, management and virtualization: An overview and open research challenges," *Wireless Pers. Commun.*, vol. 95, pp. 187–213, Jun. 2017.

[46] N. Azmi et al., "Interference issues and mitigation method in WSN 2.4 GHz ISM band: A survey," in *Proc. 2nd Int. Conf. Electron. Design (ICED)*, 2014, pp. 403–408.

[47] S. Aust, R. V. Prasad, and I. G. M. M. Niemegeers, "IEEE 802.11ah: Advantages in standards and further challenges for sub 1 GHz Wi-Fi," in *Proc. IEEE Int. Conf. Commun. (ICC)*, 2012, pp. 6885–6889.

[48] J. A. Richards, *Radio Wave Propagation: An Introduction for the Non-Specialist*. Berlin, Germany: Springer-Verlag, 2008.

[49] H. Karvonen, M. Hämäläinen, J. Iinatti, and C. Pomalaza-Ráez, "Coexistence of wireless technologies in medical scenarios," in *Proc. Eur. Conf. Netw. Commun. (EuCNC)*, 2017, pp. 1–5.

[50] R. Cavallari, F. Martelli, R. Rosini, C. Buratti, and R. Verdone, "A survey on wireless body area networks: Technologies and design challenges," *IEEE Commun. Surveys Tuts.*, vol. 16, no. 3, pp. 1635–1657, 3rd Quart., 2014.

[51] *Short Range Devices (SRD) Operating in the Frequency Range 25 MHz to 1 000 MHz; part 2: Harmonised Standard for Access to Radio Spectrum for Non Specific Radio Equipment*, ETSI Standard EN 300 220-2, 2018.

[52] S. Aust, R. V. Prasad, and I. G. Niemegeers, "Performance evaluation of sub 1 GHz wireless sensor networks for the smart grid," in *Proc. 37th Annu. IEEE Conf. Local Comput. Netw.*, 2012, pp. 292–295.

[53] S. Aras, T. Johnson, K. Cabulong, and C. Gniady, "GreenMonitor: Extending battery life for continuous heart rate monitoring in smartwatches," in *Proc. 17th Int. Conf. E-Health Netw. Appl. Services (HealthCom)*, 2015, pp. 317–322.

[54] A. Augustin, J. Yi, T. Clausen, and W. M. Townsley, "A study of LoRa: Long range & amp; low power networks for the Internet of Things," *Sensors*, vol. 16, no. 9, p. 1466, 2016. [Online]. Available: https://www.mdpi.com/1424-8220/16/9/1466

[55] M. Baert, J. Rossey, A. Shahid, and J. Hoebeke, "The Bluetooth mesh standard: An overview and experimental evaluation," *Sensors*, vol. 18, no. 8, p. 2409, 2018. [Online]. Available: https://www.mdpi.com/1424-8220/18/8/2409

[56] D. R. Gawade et al., "A museum artefact monitoring testbed using LoRaWAN," in *Proc. IEEE Symp. Comput. Commun. (ISCC)*, 2021, pp. 1–3.

[57] "HKT: SW-200 LoRaWAN smart watch." Accessed: Feb. 6, 2024. [Online]. Available: https://www.hktlora.com/product/lorawan-smart-watch/

[58] "Lilygo: T-watch S3 LoRa smartwatch." Accessed: Feb. 6, 2024. [Online]. Available: https://www.lilygo.cc/products/t-watch-s3

[59] "Origo: ED20W LoRaWAN GPS watch." Accessed: Feb. 6, 2024. [Online]. Available: http://www.origoelec.com/End-Devices/ED20W-LoRaWAN-GPS-Watch.html

[60] "Oviphone: NB-IoT-enabled smartwatches." Accessed: Feb. 6, 2024. [Online]. Available: https://www.oviphone.cn/en/nbiotshouhuanshoubiao/

[61] "kotonlink: KT-PW11 CAT M1/NB-IOT SmartWatch." Accessed: Feb. 6, 2024. [Online]. Available: https://www.kotonlink.com/KT-PW11-CAT-M1-NB-IOT-Smart-Watch-for-Workers-and-Guard-PG6764807

[62] "Sigfoc partner network: Co-assist alert watch." Accessed: Feb. 6, 2024. [Online]. Available: https://partners.sigfox.com/products/co-assist-alert-watch

[63] "Origo: ED10W LoRaWAN GPS Watch." Accessed: Feb. 6, 2024. [Online]. Available: http://www.origoelec.com/End-Devices/ED10W-LoRaWAN-GPS-Watch-for-lone-worker.html

[64] "iSmarch: J3 LoRaWAN smartwatch." Accessed: Feb. 6, 2024. [Online]. Available: https://ismarch.com/lora-watch/

[65] "Oviphone: LoRa-enabled smartwatches." Accessed: Feb. 6, 2024. [Online]. Available: https://www.oviphone.cn/en/lorashouhuanshoubiao/

[66] "Globalsat: LW-360HR LoRa GPS Tracker Watch." Accessed: Feb. 6, 2024. [Online]. Available: https://www.globalsat.com.tw/en/product-259256/LoRa-GPS-Tracker-Watch-with-Heart-Rate-Monitor-for-Senior-Health-Care-LW-360HR.html

[67] "Lilygo: T-impulse LoRa wristband." Accessed: Feb. 6, 2024. [Online]. Available: https://www.lilygo.cc/products/t-impulse-lora-wristband

[68] "Longvon: V13 NB-IoT health smart watch." Accessed: Feb. 6, 2024. [Online]. Available: https://www.longvon.com/blog/v13-nb-iot-health-smart-watch-introduction

[69] "Imyfit: NB-IoT smart watch." Accessed: Feb. 6, 2024. [Online]. Available: https://www.imyfit.com/Nb-iotWatch.html

[70] S. Kumar et al., "A bandwidth-enhanced sub-ghz wristwatch antenna using an optimized feed structure," *IEEE Antennas Wireless Propag. Lett.*, vol. 20, no. 8, pp. 1389–1393, Aug. 2021.

[71] H. M. Anderson, "Wrist watch weather radio," U.S. Patent 4 480 253, 1984.

[72] J. H. Lee, S. H. Lee, D. Kim, and C. W. Jung, "Transparent dual-band monopole antenna using a μ-metal mesh on the rear glass of an automobile for frequency modulation/digital media broadcasting service receiving," *Microw. Opt. Technol. Lett.*, vol. 61, no. 2, pp. 503–508, 2019.

[73] M.-A. Chung, "Embedded 3D multi-band antenna with ETS process technology covering LTE/WCDMA/ISM band operations in a smart wrist wearable wireless mobile communication device design," *IET Microw. Antennas Propag.*, vol. 14, no. 1, pp. 93–100, 2020.

[74] S.-W. Su and Y.-T. Hsieh, "Integrated LDS antenna for B13 and B4/B3/B2/B1 LTE operation in smartwatch," *Microw. Opt. Technol. Lett.*, vol. 59, no. 4, pp. 869–873, 2017.

[75] S. Kumar et al., "A 915 MHz wristwatch-integrated antenna for wireless health monitoring," in *Proc. 14th Eur. Conf. Antennas Propag. (EuCAP)*, 2020, pp. 1–5.

[76] X. Gao, Z. Zhang, W. Chen, Z. Feng, M. F. Iskander, and A.-P. Zhao, "A novel wristwear dual-band diversity antenna," in *Proc. IEEE Antennas Propag. Soc. Int. Symp.*, 2009, pp. 1–4.

[77] S. Kumar et al., "A bandwidth enhanced 915 MHz antenna for IoT wrist-watch applications," in *Proc. 13th Eur. Conf. Antennas Propag. (EuCAP)*, 2019, pp. 1–5.

[78] H. Hamouda, P. Le Thuc, R. Staraj, and G. Kossiavas, "Dualband MICS/WiFi small antenna for portable applications in telemedicine," in *Proc. IEEE Antennas Propag. Soc. Int. Symp. (APSURSI)*, 2013, pp. 2081–2082.

[79] L. Catarinucci, F. P. Chietera, and R. Colella, "Permittivity-customizable ceramic-doped silicone substrates shaped with 3-D-printed molds to design flexible and conformal antennas," *IEEE Trans. Antennas Propag.*, vol. 68, no. 6, pp. 4967–4972, Jun. 2020.

[80] W.-H. Ng, Y.-H. Lee, E.-H. Lim, and B.-K. Chung, "Design of a compact PIFA tag antenna for wearable electronics," in *Proc. IEEE 38th Int. Electron. Manuf. Technol. Conf. (IEMT)*, 2018, pp. 1–4.

[81] J. Chen, M. Berg, V. Somero, H. Y. Amin, and A. Pärssinen, "A multiple antenna system design for wearable device using theory of characteristic mode," in *Proc. 12th Eur. Conf. Antennas Propag. (EuCAP)*, 2018, pp. 1–5.

[82] J. Chen, M. Berg, H. Y. Amin, and A. Pärssinen, "Effect of small wearable device antenna location on its impedance, bandwidth potential and radiation efficiency," in *Proc. Loughborough Antennas Propag. Conf. (LAPC)*, 2017, pp. 1–5.

[83] J. R. Flores-Cuadras, J. L. Medina-Monroy, R. A. Chavez-Perez, and H. Lobato-Morales, "Novel ultra-wideband flexible antenna for wearable wrist worn devices with 4G LTE communications," *Microw. Opt. Technol. Lett.*, vol. 59, no. 4, pp. 777–783, 2017.

[84] K. Zhao, Z. Ying, and S. He, "Antenna designs of smart watch for cellular communications by using metal belt," in *Proc. 9th Eur. Conf. Antennas Propag. (EuCAP)*, 2015, pp. 1–5.

[85] T. Pumpoung, P. Wongsiritorn, C. Phongcharoenpanich, and S. Kosulvit, "UHF-RFID tag antenna using t-matching and double-ended rectangular loop techniques for wristband applications," in *Proc. Theory Appl. Appl. Electromagn. (APPEIC)*, 2016, pp. 97–107.

[86] M.-T. Nguyen, Y.-F. Lin, C.-H. Chen, Y.-C. Tseng, and H.-M. Chen, "Miniature 3-D-dipole antenna for UHF RFID tag mounted on conductive materials," *IEEE Trans. Antennas Propag.*, vol. 70, no. 12, pp. 11454–11464, Dec. 2022.

[87] M.-T. Nguyen, Y.-F. Lin, C.-H. Chen, C.-C. Chang, and H.-M. Chen, "Low-profile wideband miniaturized tag antenna mounted on the human body," *Int. J. Microw. Wireless Technol.*, to be published.

[88] C.-T. Liao, Z.-K. Yang, and H.-M. Chen, "Multiple integrated antennas for wearable fifth-generation communication and Internet of Things applications," *IEEE Access*, vol. 9, pp. 120328–120346, 2021.

[89] J.-Y. Park and J.-M. Woo, "Microstrip line monopole antenna for the wearable applications," in *Proc. 38th Eur. Microw. Conf.*, 2008, pp. 1277–1279.

[90] J.-Y. Park and J.-M. Woo, "Miniaturization of microstrip line monopole antenna for the wearable applications," in *Proc. Asia–Pac. Microw. Conf.*, 2008, pp. 1–4.

[91] C.-Y. Hong and S.-H. Yeh, "Cellular antenna design with metallic housing for wearable device," in *Proc. IEEE 5th Asia–Pac. Conf. Antennas Propag. (APCAP)*, 2016, pp. 419–420.

[92] Y. Jia, L. Liu, J. Hu, and L.-J. Xu, "Miniaturized wearable watch antenna for wristband applications," in *Proc. IEEE MTT-S Int. Microw. Biomed. Conf. (IMBioC)*, vol. 1, 2019, pp. 1–3.

[93] B. Xu, Y. Li, and Y. Kim, "Classification of finger movements based on reflection coefficient variations of a body-worn electrically small antenna," *IEEE Antennas Wireless Propag. Lett.*, vol. 16, pp. 1812–1815, 2017.

[94] S. Lopez-Soriano and J. Parron, "Design of a small-size, low-profile, and low-cost normal-mode helical antenna for UHF RFID wristbands," *IEEE Antennas Wireless Propag. Lett.*, vol. 16, pp. 2074–2077, 2017.

[95] D. Wang, Y. J. Zhang, and M. S. Tong, "A wearable UHF RFID tag antenna with archimedean spiral strips," in *Proc. IEEE Progr. Electromagn. Res. Symp. Fall (PIERS-FALL)*, 2017, pp. 1849–1852.

[96] Y. Kong, B. Wang, and H. Li, "Compact and dual-band antenna for smartwatch application," in *Proc. IEEE 4th Int. Conf. Electron. Inf. Commun. Technol. (ICEICT)*, 2021, pp. 856–858.

[97] A. Semenov, O. Semenova, P. Bogdan, R. Kulias, and O. Shpylovyi, "Development of a flexible antenna-wristband for wearable wrist-worn infocommunication devices of the LTE standard," *Technol. Audit Prod. Reserves*, vol. 1, no. 65, pp. 20–26, 2022.

[98] G.-L. Huang, C.-Y.-D. Sim, S.-Y. Liang, W.-S. Liao, and T. Yuan, "Low-profile flexible UHF RFID tag design for wristbands applications," *Wireless Commun. Mobile Comput.*, vol. 2018, Jun. 2018, Art. no. 9482919.

[99] S. López-Soriano and J. Parrón, "Wearable RFID tag antenna for healthcare applications," in *Proc. IEEE-APS Topical Conf. Antennas Propag. Wireless Commun. (APWC)*, 2015, pp. 287–290.

[100] W.-S. Chen, G.-Q. Lin, G.-R. Zhang, and C.-Y.-D. Sim, "Multiband antennas for GSM/GPS/LTE/WLAN smart watch applications," in *Proc. 6th Asia–Pac. Conf. Antennas Propag. (APCAP)*, 2017, pp. 1–3.

[101] Y. Tang, L. Jia, H. Zhang, and B. Liu, "Internal digital video broadcasting-handheld antenna with a low loss z-type hexaferrite for folder-type mobile phones," *Microw. Opt. Technol. Lett.*, vol. 54, no. 6, pp. 1380–1385, 2012.

[102] J.-H. Lu, J.-H. Zhuang, and J.-W. Hsu, "A smartwatch dipole antenna for LTE/GPS/WWAN applications," in *Proc. Int. Symp. Antennas Propag. (ISAP)*, 2018, pp. 1–2.

[103] J.-H. Lu, J.-W. Hsu, and J.-H. Zhuang, "A LTE/GPS/WWAN dipole antenna for smartwatch applications," in *Proc. Asia–Pac. Microw. Conf. (APMC)*, 2018, pp. 1606–1608.

[104] F. Z. Marouf and D. Ziani Kerarti, "Study and design of wristband RFID antenna for healthcare applications," *Microw. Opt. Technol. Lett.*, vol. 60, no. 2, pp. 359–364, 2018.

[105] G. R. Hoch, P. Nayeri, and A. Elsherbeni, "Bandwidth enhancement of dipole antennas using parasitic elements," in *Proc. 31st Int. Rev. Progr. Appl. Comput. Electromagn. (ACES)*, 2015, pp. 1–2.

[106] C. Laohapensaeng, C. Free, and K. Lum, "Printed strip monopole antenna with the parasitic elements on the circular ground plane," in *Proc. IEEE Int. Workshop Antenna Technol. Small Antennas Novel Metamater. (IWAT)*, 2005, pp. 371–374.

[107] "ICNIRP guidelines for limiting exposure to electromagnetic fields (100 KHz to 300 GHz." 2020. [Online]. Available: https://www.icnirp.org/en/activities/news/news-article/rf-guidelines-2020-published.html#:~:text=The%20ICNIRP%20Guidelines%20on%20Limiting,mobile%20phones%2C%20and%20base%20stations

[108] *Evaluating Compliance With FCC Guidelines for Human Exposure to Radio Frequency Electromagnetic Fields, Supplement c (Edition 01-01) to OET Bulletin 65 (Edition 97-01)*, Fed. Commun. Commission, Washington, DC, USA, 2001.

[109] C. G. Akagündüz and E. Soylemez, "Optimization of laser direct structuring process parameters for material extrusion of polycarbonate," *Adv. Eng. Mater.*, vol. 25, no. 23, 2023, Art. no. 2300907.

[110] S. Kumar, J. L. Buckley, A. Di Serio, and B. O'Flynn, "Comparative analysis of circuit and finite element models for a linear wire dipole antenna," in *Proc. 29th Irish Signals Syst. Conf. (ISSC)*, 2018, pp. 1–6.

[111] H. T. Chattha, Y. Huang, Y. Lu, and X. Zhu, "Further bandwidth enhancement of PIFA by adding a parasitic element," in *Proc. Loughborough Antennas Propag. Conf.*, 2009, pp. 213–216.

[112] N. S. Khamaruzaman, M. Jusoh, T. Sabapathy, M. N. Osman, S. Subahir, and M. H. Jamaluddin, "Wearable UHF RFID antenna based metamaterial," in *Proc. IEEE Asia–Pac. Conf. Appl. Electromagn. (APACE)*, 2021, pp. 1–5.

[113] *IEEE Recommended Practice for Measurements and Computations of Radio Frequency Electromagnetic Fields With Respect to Human Exposure to Such Fields, 100 kHz–300 GHz*, IEEE Standard C95.3-2002, 2002.

[114] B. O'Callaghan, D. R. Gawade, S. Kumar, D. O'Hare, and J. L. Buckley, "A time-efficient model for estimating far-field wireless power transfer to biomedical implants," in *Proc. 18th Eur. Conf. Antennas Propag. (EuCAP)*, 2024, pp. 1–5.

[115] *IEEE Standard for Safety Levels With Respect to Human Exposure to Radio Frequency Electromagnetic Fields, 3 kHz to 300 GHz*, IEEE Standard C95.1-2019, 1999.

[116] *IEEE Standard for Low-Rate Wireless Networks*, IEEE Standard 802.15.4-2020, 2016.

[117] C. A. Balanis, *Antenna Theory: Analysis and Design*. Hoboken, NJ, USA: Wiley, 2016.

[118] S. Kumar, *Bandwidth Enhanced Sub-GHZ Wristwatch Antennas for Wireless Body Sensor Network Applications*, Univ. College Cork, Cork, Ireland, 2021.

[119] C. Pfeiffer, "Fundamental efficiency limits for small metallic antennas," *IEEE Trans. Antennas Propag.*, vol. 65, no. 4, pp. 1642–1650, Apr. 2017.

[120] C. Song et al., "Matching network elimination in broadband rectennas for high-efficiency wireless power transfer and energy harvesting," *IEEE Trans. Ind. Electron.*, vol. 64, no. 5, pp. 3950–3961, May 2017.

[121] M. Lauridsen, B. Vejlgaard, I. Z. Kovacs, H. Nguyen, and P. Mogensen, "Interference measurements in the European 868 MHz ISM band with focus on LoRa and SigFox," in *Proc. IEEE Wireless Commun. Netw. Conf. (WCNC)*, 2017, pp. 1–6.

[122] "LoRa Alliance: RP002-1.0.2 LoRaWAN regional parameters." Accessed: Feb. 10, 2024. [Online]. Available: https://www.thethingsnetwork.org/docs/lorawan/frequencies-by-country/

[123] P. Pongpaibool, "A study on performance of UHF RFID tags in a package for animal traceability application," in *Proc. 5th Int. Conf. Elect. Eng. Electron. Comput. Telecommun. Inf. Technol.*, vol. 2, 2008, pp. 741–744.

[124] H. J. M. Vincent, "Placement of an antenna in a wrist worn device," U.S. Patent 9 602 642, Mar. 21, 2017.

[125] A. Zandamela, N. Marchetti, and A. Narbudowicz. "Directional modulation for enhanced privacy in smart watch devices." 2023. [Online]. Available: https://www.techrxiv.org/doi/full/10.36227/techrxiv.24517240.v1

[126] A. Zandamela, N. Marchetti, M. J. Ammann, and A. Narbudowicz, "3D beam-steering MIMO antenna for on-body IoT applications," *IEEE Trans. Antennas Propag.*, vol. 72, no. 3, pp. 2241–2251, Mar. 2024.

[127] T. Wu, D. Qu, and G. Zhang, "Research on LoRa adaptability in the leo satellites Internet of Things," in *Proc. 15th Int. Wireless Commun. Mobile Comput. Conf. (IWCMC)*, 2019, pp. 131–135.

[128] M. R. Palattella and N. Accettura, "Enabling Internet of Everything everywhere: LPWAN with satellite backhaul," in *Proc. Global Inf. Infrastruct. Netw. Symp. (GIIS)*, 2018, pp. 1–5.

[129] M. Fallahpour and R. Zoughi, "Antenna miniaturization techniques: A review of topology- and material-based methods," *IEEE Antennas Propag. Mag.*, vol. 60, no. 1, pp. 38–50, Feb. 2018.

[130] W. Li, D. Li, K. Zhou, Q. Fu, X. Yuan, and X. Zhu, "A survey of antenna miniaturization technology based on the new mechanism of acoustic excitation," *IEEE Trans. Antennas Propag.*, vol. 71, no. 1, pp. 263–274, Jan. 2023.

[131] C. A. Lynch, A. Eid, Y. Fang, and M. M. Tentzeris, "Inkjet-/3D-/4D-printed 'zero-power' flexible wearable wireless modules for smart biomonitoring and pathogen sensing," in *Proc. IEEE Int. Conf. Flexible Printable Sensors Syst. (FLEPS)*, 2021, pp. 1–3.

[132] S. Tansaz, A. Baronetto, R. Zhang, A. Derungs, and O. Amft, "Printing wearable devices in 2D and 3D: An overview on mechanical and electronic digital co-design," *IEEE Pervasive Comput.*, vol. 18, no. 4, pp. 38–50, Oct.–Dec. 2019.

[133] J. Persad and S. Rocke, "A survey of 3D printing technologies as applied to printed electronics," *IEEE Access*, vol. 10, pp. 27289–27319, 2022.

[134] L. Engel et al., "3D printed hemispherically radiating antenna for broadband millimeter wave applications," *IEEE Open J. Antennas Propag.*, vol. 4, pp. 558–570, 2023.

[135] R. B. V. B. Simorangkir et al., "Screen printed epidermal antenna for IoT health monitoring," in *Proc. IEEE Asia–Pac. Microw. Conf. (APMC)*, 2021, pp. 395–397.

[136] D. R. Gawade et al., "A battery-less NFC sensor transponder for cattle health monitoring," in *Proc. IEEE Appl. Sens. Conf. (APSCON)*, 2023, pp. 1–3.

[137] U. Ali, S. Ullah, B. Kamal, L. Matekovits, and A. Altaf, "Design, analysis and applications of wearable antennas: A review," *IEEE Access*, vol. 11, pp. 14458–14486, 2023.

[138] G. Moloudian et al., "RF energy harvesting techniques for battery-less wireless sensing, industry 4.0 and Internet of Things: A review," *IEEE Sensors J.*, vol. 24, no. 5, pp. 5732–5745, Mar. 2024.

[139] S. Liu, B. Xue, W. Yan, A. Y. Rwei, and C. Wu, "Recent advances and design strategies towards wearable near-infrared spectroscopy," *IEEE Open J. Nanotechnol.*, vol. 4, pp. 25–35, 2023.

[140] M. M. Khan, S. Hossain, P. Mozumdar, S. Akter, and R. H. Ashique, "A review on machine learning and deep learning for various antenna design applications," *Heliyon*, vol. 8, no. 4, 2022, Art. no. e09317.

[141] N. Rather, R. B. V. B. Simorangkir, J. L. Buckley, B. O'Flynn, and S. Tedesco, "Deep-learning-assisted robust detection techniques for a chipless RFID sensor tag," *IEEE Trans. Instrum. Meas.*, vol. 73, pp. 1–10, 2024.

[142] D. Pal, R. Singhal, and A. K. Bandyopadhyay, "Parametric optimization of complementary split-ring resonator dimensions for planar antenna size miniaturization," *Wireless Pers. Commun.*, vol. 123, no. 2, pp. 1897–1911, 2022.

[143] G. Moloudain, S. Kumar, B. O'Flynn, and J. L. Buckley, "A compact microwave rectifier for wireless power transfer and energy harvesting applications," in *Proc. 18th Eur. Conf. Antennas Propag. (EuCAP)*, 2024, pp. 1–4.

[144] "PowerSpot power-over-distance wireless transmitter." Accessed: Feb. 8, 2024. [Online]. Available: https://www.powercastco.com/powercast-ships-powerspot-power-distance-wireless-transmitter/

[145] "Powercast." Accessed: Feb. 8, 2024. [Online]. Available: https://www.powercastco.com/

[146] R. B. V. B. Simorangkir et al., "Transparent epidermal antenna for unobtrusive human-centric Internet of Things applications," *IEEE Internet Things J.*, vol. 11, no. 1, pp. 1164–1174, Jan. 2024.

[147] A. S. M. Sayem et al., "Flexible transparent antennas: Advancements, challenges, and prospects," *IEEE Open J. Antennas Propag.*, vol. 3, pp. 1109–1133, 2022.

[148] A. R. Chishti et al., "Optically transparent antennas: A review of the state-of-the-art, innovative solutions and future trends," *Appl. Sci.*, vol. 13, no. 1, p. 210, 2022.

[149] Y. Morimoto, S. Shiu, I. W. Huang, E. Fest, G. Ye, and J. Zhu, "Optically transparent antenna for smart glasses," *IEEE Open J. Antennas Propag.*, vol. 4, pp. 159–167, 2023.

[150] J. Park, S. Y. Lee, J. Kim, D. Park, W. Choi, and W. Hong, "An optically invisible antenna-on-display concept for millimeter-wave 5G cellular devices," *IEEE Trans. Antennas Propag.*, vol. 67, no. 5, pp. 2942–2952, May 2019.

[151] A. D. Tadesse, O. P. Acharya, and S. Sahu, "Application of metamaterials for performance enhancement of planar antennas: A review," *Int. J. RF Microw. Comput.-Aided Eng.*, vol. 30, no. 5, 2020, Art. no. e22154.

[152] Y.-S. Chen and T.-Y. Ku, "A low-profile wearable antenna using a miniature high impedance surface for smartwatch applications," *IEEE Antennas Wireless Propag. Lett.*, vol. 15, pp. 1144–1147, 2016.

[153] D. Wen, Y. Hao, H. Wang, and H. Zhou, "A wearable antenna design using a high impedance surface for all-metal smartwatch applications," in *Proc. Int. Workshop Antenna Technol. Small Antennas Innov. Struct. Appl. (iWAT)*, 2017, pp. 274–276.

[154] T.-Y. Ku and Y.-S. Chen, "Wearable antenna design on finite-size high impedance surfaces for smart-watch applications," in *Proc. IEEE Int. Symp. Antennas Propag. USNC/URSI Nat. Radio Sci. Meeting*, 2015, pp. 938–939.

[155] R. Rabhi, S. Gahgouh, and A. Gharsallah, "Watchstrap integrated wideband circularly polarized antenna design for smartwatch applications," *IET Microw. Antennas Propag.*, vol. 16, no. 9, pp. 587–601, 2022.

[156] W. Zheng, H. Li, and G. Liu, "Design of circularly polarized smartwatch antenna with reactive loads," *IEEE Antennas Wireless Propag. Lett.*, vol. 22, no. 7, pp. 1602–1606, Jul. 2023.

[157] A. K. Pandey, N. K. Sahu, R. K. Gangwar, and R. K. Chaudhary, "SIW-cavity-backed wideband circularly polarized antenna using modified split-ring slot as a radiator for mm-wave IoT applications," *IEEE Internet Things J.*, vol. 11, no. 7, pp. 11793–11799, Apr. 2024.

SANJEEV KUMAR (Member, IEEE) received the B.Tech. degree in electronics and communications engineering from the Sam Higginbottom University of Agriculture, Technology and Sciences, Prayagraj, India, in 2012, the M.S. by Research degree in electronics and communications engineering from The LNM Institute of Information Technology, Jaipur, India, in 2015, and the Ph.D. degree in electrical and electronic engineering from University College Cork, Cork, Ireland, in 2021.

From 2012 to 2013, he worked as an RF Engineer with Wipro, Mumbai, India. From 2015 to 2016, he was an Assistant Professor with the Department of Electronics and Communication Engineering, Pratap Institute of Technology and Science, Sikar, India. Since February 2022, he has been a Postdoctoral Researcher with the Wireless Sensor Networks Group, Tyndall National Institute, University College Cork. His research interests include the design and development of electrically small antennas, wearable and implantable antennas, NFC and RFID, RF energy harvesting, wireless charging, circuit modeling, embedded hardware PCB design, and the exploration of nonconventional materials for the advancement of next-generation antennas and sensing systems. He serves as a reviewer for several top-tier international journals and conferences in the field of antennas and propagation.

GHOLAMHOSEIN MOLOUDIAN (Member, IEEE) received the Associate's degree (Highest GPA, First-Class Hons.) in electronic and electrical engineering from Technical and Vocational University, Yasouj, Iran, in 2008, the B.Sc. degree in electronic and electrical engineering from Higher Education Center, Shiraz, Iran, in 2010, the M.Sc. degree (Highest GPA, First-Class Hons.) in electronic and electrical engineering from Islamic Azad University (IAU) of Bushehr, Bushehr, Iran, in 2012, and the Ph.D. degree (Hons.) in electronic and electrical engineering from IAU (Arak Branch), Arak, Iran, in 2018.

He worked as a Researcher and a Lecturer with the Department of Electrical Engineering, Salman Farsi University of Kazerun, Kazerun, Iran, and the IAU of Kazerun, Kazerun, Iran, from January 2016 to September 2020. Moreover, he worked with the South Electrical Management Company in the field of industrial sensors and energy efficiency from October 2020 to December 2021. He is currently working with the Wireless Sensor Networks Group (Antenna/RF Team), Tyndall National Institute, University College Cork, Cork, Ireland, as a Marie Skłodowska-Curie (MSCA) Research Fellow and a SMART 4.0 Fellow (with the SFI-CONFIRM Center). His research interests include design and analysis of RF/microwave circuits, wireless power transfer, energy harvesting, RF MEMS, RF low-power electronic circuits, PCB design, RFID, and microstrip antennas and sensors. He is a reviewer for several top-tier IEEE, MDPI, and Elsevier journals. He served as the main Guest Editor for *Electronics* (MDPI) and a Guest Editor for *IET Microwaves, Antennas & Propagation*, Special Issues on Trends and Prospects: RF/Microwave and MM-Wave Circuits and Systems. He was granted the prestigious MSCA Fellowship (SMART Industry 4.0 Program) to further his research on battery-less wireless sensing and monitoring systems for Internet of Things and Industry 4.0 applications.

ROY B. V. B. SIMORANGKIR (Member, IEEE) received the B.S. degree in telecommunication engineering from Institut Teknologi Bandung, Indonesia, in 2010, the M.S. degree in electrical and electronic engineering from Yonsei University, South Korea, in 2014, and the Ph.D. degree in electronic engineering from Macquarie University, Australia, in 2018. After completing his Ph.D., he pursued postdoctoral research with Macquarie University; the Institute of Electronics and Telecommunications of Rennes, France; and Tyndall National Institute, Ireland. He is currently an Assistant Professor with the Department of Engineering, Durham University, U.K., where he specializes in the development of unconventional materials-based antennas and sensors for next-generation wireless communication and sensing systems. He has published over 60 refereed research papers in this field, including award-winning work. He has also taken on leadership roles at major international conferences and received recognition as an outstanding reviewer for esteemed journals, notably from 2021 to 2023 for the IEEE TRANSACTIONS ON ANTENNAS AND PROPAGATION.

DINESH R. GAWADE (Graduate Student Member, IEEE) received the Bachelor of Technology degree in electronics and communication technology from the Department of Technology, Shivaji University, India, in 2016, and the M.Eng.Sc. degree from the Tyndall National Institute, University College Cork, Cork, Ireland, in 2022. He is currently pursuing the Ph.D. degree with the Tyndall National Institute and Microelectronic Circuit Centre Ireland, Cork. Following his graduation, he gained valuable industry experience as a Hardware Design Engineer from 2016 to 2018. Subsequently, he contributed his expertise to the Indian Institute of Technology Mandi, Mandi, India, as a Project Engineer specializing in Hardware Design. In 2019, he joined the Tyndall National Institute, University College Cork, to further advance his research and career. His research interests encompass a broad range of topics, including the development of battery-less sensing devices, radio-frequency integrated circuit design, antenna design, low-power sensor node design, and design of long-range wireless sensor network for various application.

BRENDAN O'FLYNN (Senior Member, IEEE) received the B.Eng. (Hons.), M.Eng.Sc., and Ph.D. degrees from University College Cork, Cork, Ireland, where he is currently a Senior Staff Researcher with Tyndall National Institute. He is also the Head of the Wireless Sensor Networks Group. His research interests include wearable sensing systems, edge-based analytics, sensor system integration, low-power embedded systems design and development, system miniaturization, and RF system design and optimization. He has published widely in these areas and has secured significant funding for the development and deployment of "smart sensing" technologies and applied research projects.

JOHN L. BUCKLEY (Member, IEEE) was born in Cork, Ireland. He received the B.Eng. degree from the Cork Institute of Technology, Cork, in 1994, and the M.Eng.Sc. and Ph.D. degrees from the Department of Electrical and Electronic Engineering, University College Cork (UCC), Cork, in 2004 and 2016, respectively. From 1994 to 2002, he was with EMC Corporation, Cork, where he specialized in printed-circuit board design, high-speed digital design, and signal integrity. He joined the Tyndall National Institute, UCC, in 2005, where he is currently a Senior Researcher and leads the Antenna and RF Team's research activities working on both fundamental and applied antenna and RF research. He has published more than 80 scientific works and acts as a reviewer for several international antenna journals and conferences in the field of antennas and propagation. His research interests include electrically small antenna design, tunable antennas, wearable and implantable antennas, and RF front-end design. He served as the General Co-Chair for the International Conference on Antenna Technology (iWAT) in 2022.